



Article

In Silico Studies of Some Isoflavonoids as Potential Candidates against COVID-19 Targeting Human ACE2 (hACE2) and Viral Main Protease (M^{Pro})

Mohamed S. Alesawy ^{1,*} , Abdallah E. Abdallah ¹, Mohammed S. Taghour ¹ , Eslam B. Elkaeed ^{2,3} , Ibrahim H. Eissa ^{1,*}  and Ahmed M. Metwaly ⁴ 

¹ Medicinal Pharmaceutical Chemistry & Drug Design Department, Faculty of Pharmacy (Boys), Al-Azhar University, Cairo 11884, Egypt; Abdulla_emara@azhar.edu.eg (A.E.A.); Mohammad1533.el@azhar.edu.eg (M.S.T.)

² Department of Pharmaceutical Sciences, College of Pharmacy, AlMaarefa University, Ad Diriyah, Riyadh 13713, Saudi Arabia; ikaeed@mcst.edu.sa

³ Department of Pharmaceutical Organic Chemistry, Faculty of Pharmacy (Boys), Al-Azhar University, Cairo 11884, Egypt

⁴ Department of Pharmacognosy and Medicinal Plants, Faculty of Pharmacy (Boys), Al-Azhar University, Cairo 11884, Egypt; ametwaly@azhar.edu.eg

* Correspondence: mohammedalesawy@azhar.edu.eg (M.S.A.); Ibrahimeissa@azhar.edu.eg (I.H.E.)



Citation: Alesawy, M.S.; Abdallah, A.E.; Taghour, M.S.; Elkaeed, E.B.; H. Eissa, I.; Metwaly, A.M. In Silico Studies of Some Isoflavonoids as Potential Candidates against COVID-19 Targeting Human ACE2 (hACE2) and Viral Main Protease (M^{Pro}). *Molecules* **2021**, *26*, 2806. <https://doi.org/10.3390/molecules26092806>

Academic Editors: Teobald Kupka and Baoan Song

Received: 22 March 2021

Accepted: 25 April 2021

Published: 10 May 2021

Publisher's Note: MDPI stays neutral with regard to jurisdictional claims in published maps and institutional affiliations.



Copyright: © 2021 by the authors. Licensee MDPI, Basel, Switzerland. This article is an open access article distributed under the terms and conditions of the Creative Commons Attribution (CC BY) license (<https://creativecommons.org/licenses/by/4.0/>).

Abstract: The Severe acute respiratory syndrome coronavirus 2 (SARS-CoV-2) caused the “COVID-19” disease that has been declared by WHO as a global emergency. The pandemic, which emerged in China and widespread all over the world, has no specific treatment till now. The reported antiviral activities of isoflavonoids encouraged us to find out its in silico anti-SARS-CoV-2 activity. In this work, molecular docking studies were carried out to investigate the interaction of fifty-nine isoflavonoids against hACE2 and viral M^{Pro}. Several other in silico studies including physicochemical properties, ADMET and toxicity have been preceded. The results revealed that the examined isoflavonoids bound perfectly the hACE-2 with free binding energies ranging from -24.02 to -39.33 kcal mol⁻¹, compared to the co-crystallized ligand (-21.39 kcal mol⁻¹). Furthermore, such compounds bound the M^{Pro} with unique binding modes showing free binding energies ranging from -32.19 to -50.79 kcal mol⁻¹, comparing to the co-crystallized ligand (binding energy = -62.84 kcal mol⁻¹). Compounds **33** and **56** showed the most acceptable affinities against hACE2. Compounds **30** and **53** showed the best docking results against M^{Pro}. In silico ADMET studies suggest that most compounds possess drug-likeness properties.

Keywords: COVID-19; isoflavonoids; molecular docking; human ACE2; main protease

1. Introduction

In December 2019, an outbreak of severe pneumonia caused by the novel severe SARS-CoV-2 originated in Wuhan, China. The infection spread all over the world causing coronavirus disease (COVID-19) [1,2]. By October 2020, COVID-19 caused more than 33 million infections and more than 1 million deaths according to the WHO [3]. Unfortunately, till now there is no specific antiviral drug available for the treatment of COVID-19-infected people. However, some drugs such as remdesivir showed modest activity through decreasing the mortality rate and treatment time [4].

M^{Pro} is an essential non-structural chymotrypsin-like cysteine proteases enzyme for the replication of coronavirus. It works on two large polyproteins (PP1a and PP1ab) releasing 16 essential non-structural proteins (NSPs 1-16) [5,6].

Angiotensin-converting enzyme (ACE-2) is a crucial enzyme in the renin-angiotensin system. It is a significant target for antihypertensive drugs [7]. It is primarily expressed in renal tubular epithelium and vascular endothelium cells [8]. It was also reported to be

expressed in lungs and GIT, tissues shown to harbor SARS-CoV [9,10]. The binding of SARS-CoV-2 to ACE-2 receptors was reported to play a pivotal role in the first binding step at the cellular membrane [11]. SARS-CoV-2 entry was mediated by its transmembrane spike glycoprotein [12]. ACE-2 was identified as the cellular receptor to which spike glycoprotein of SARS-CoV-2 binds [13]. Several reports confirmed that the SARS-CoV-2 infects human cells through ACE-2 receptor [11,14]. Furthermore, it was found that the overexpression of ACE-2 in a living cell facilitates virus entry [15].

Natural secondary metabolites are a major source of anti-infective drugs. These metabolites could be originated from plants [16,17], marine [18,19], or microbial sources [20–22], and found to belong to various types such as saponins [23,24], alkaloids [25], pyrones [26], isochromenes [27], diterpenes [28], flavonoids [29,30], and isoflavonoids [31].

The isoflavonoids are an important polyphenolic subclass of the flavonoids with a skeleton based on a 3-phenylchroman structure [32]. The antiviral power of several isoflavonoid secondary metabolites has been proven in several scientific reports before. Torvanol A is a sulfated isoflavonoid isolated from the fruits of *Solanum torvum* and exhibited antiviral activity against herpes simplex virus type 1 with an IC_{50} value of $9.6 \mu\text{g mL}^{-1}$ [33]. Genistein; the major isoflavonoid of soybean seeds inhibited HSV-1 (KOS and 29R strains), and HSV-2 (333 strain) replications with IC_{50} values of 14.02, 7.76 and 14.12, respectively. In addition, three isoflavone glycosides were obtained from some hypocotyls of soybean seeds and could completely inhibit HIV-induced cytopathic effects and virus-specific antigen expression just six days after infection at a concentration of 0.25 mg mL^{-1} [34]. Daidzein was reported to inhibit the influenza virus at an IC_{50} of $51.2 \mu\text{M}$ [35].

Furthermore, homoisoflavonoids showed great antiviral activity against the enteroviruses, Coxsackievirus B1, B3, B4, A9 and echovirus 30 [36]. Interestingly, a group of synthesized substituted homo-isoflavonoids exhibited promising inhibitory effects against human rhinovirus (HRV) 1B and 14 [37]. These findings inspired us to explore the potential of fifty-nine isoflavonoids (1–59) (Figure 1) as a possible treatment for COVID-19 through in silico examination of their potential to bind with ACE-2 and M^{pro} receptors.

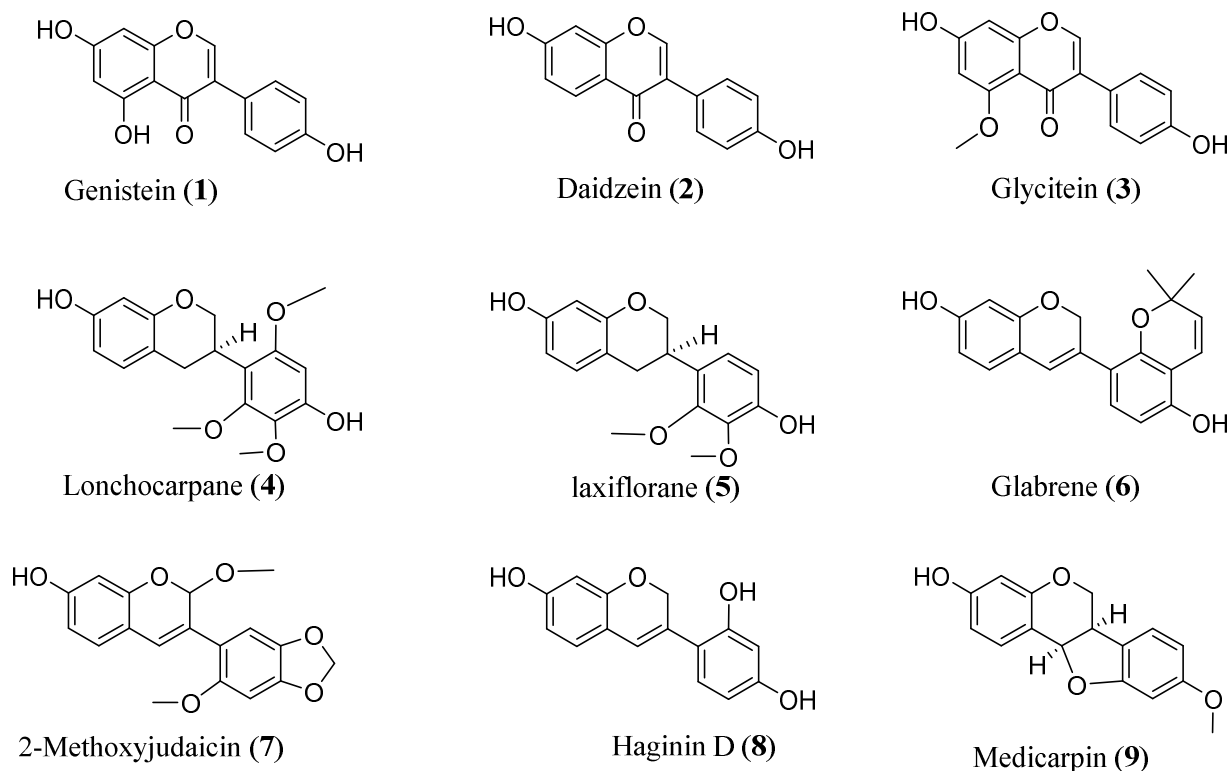


Figure 1. Cont.

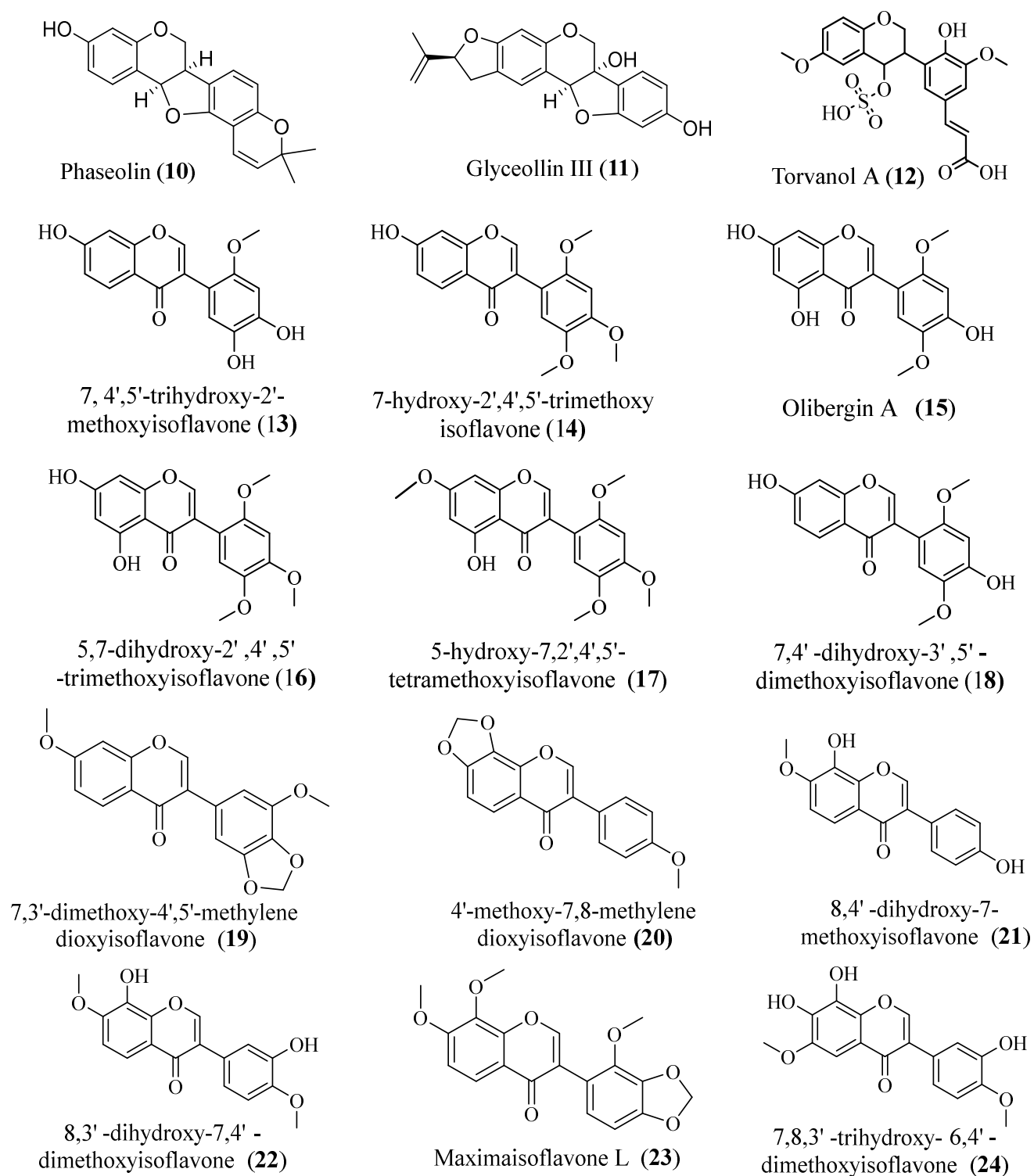


Figure 1. Cont.

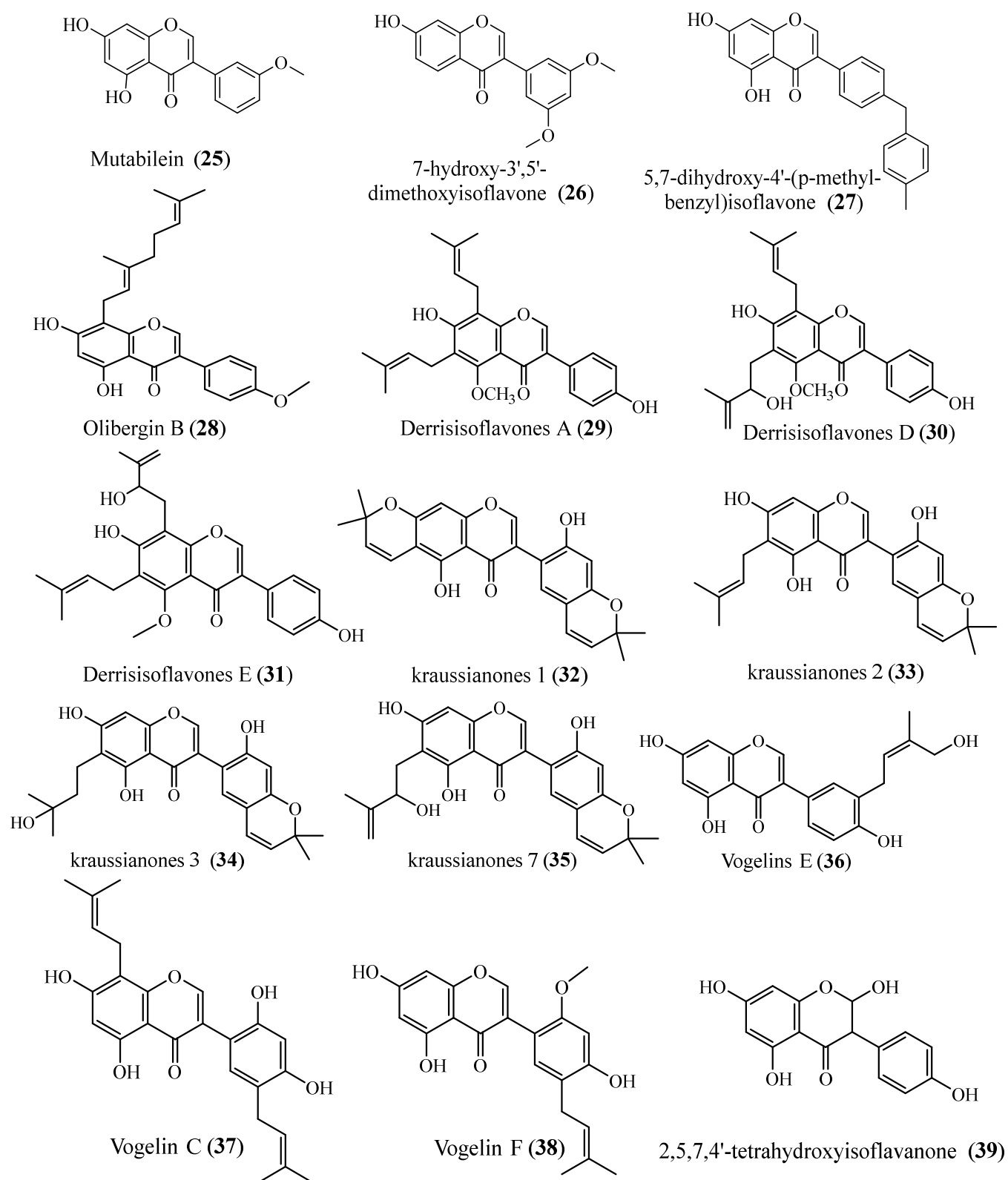


Figure 1. Cont.

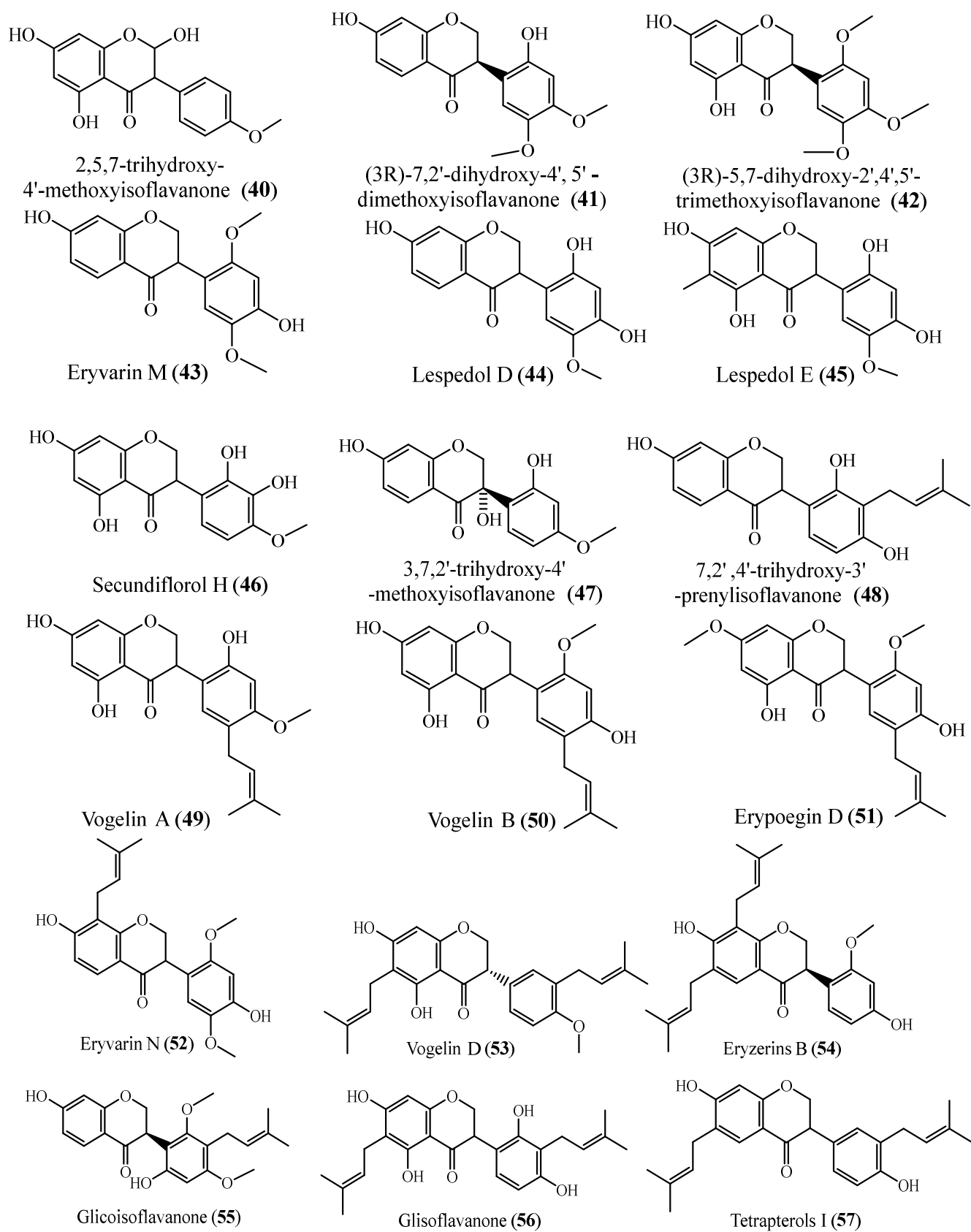


Figure 1. Cont.

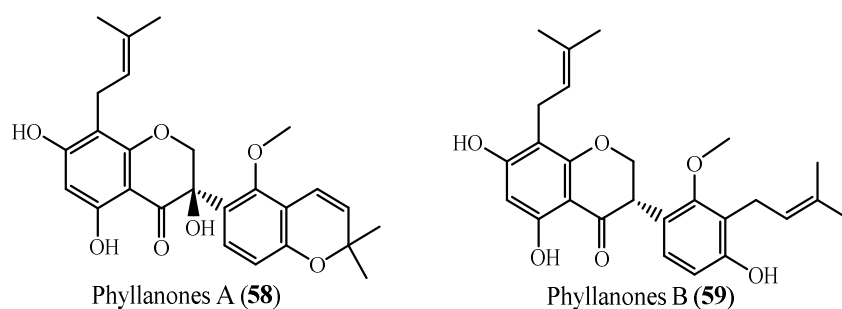


Figure 1. Structures of the examined isoflavonoids.

2. Experimental

Drug-likeness properties were calculated using Lipinski's rule of five, which suggested that the absorption of an orally administered compound is more likely to be better if the molecule satisfies at least three of the following rules: (i) H bond donors (OH, NH, and SH) ≤ 5 ; (ii) H bond acceptors (N, O, and S atoms) ≤ 10 ; (iii) molecular weight < 500 ; (iv) $\log P < 5$. Compounds violating more than one of these rules could not have good oral bioavailability [38]. The pharmacokinetic properties (ADMET) of isoflavonoids and adherence with Lipinski's rule of five were calculated using Discovery studio 4.0 software (Accelrys software Inc., San Diego, CA, USA) [39].

The title molecules were investigated with the aid of docking studies using *Discovery Studio 4.0* software (Accelrys software Inc., San Diego, CA, USA) for their binding capabilities against ACE-2 and M^{Pro} . The crystal structures of the target proteins were acquired from the RCSB Protein Data Bank (PDB ID: 6LZG, resolution: 2.50 Å [40] and 6LU7, resolution: 2.16 Å [41] for ACE-2 and M^{Pro} , respectively). The co-crystallized ligands 2-acetamido-2-deoxy- β -D-glucopyranose (NAG) and *N*-[(5-methylisoxazol-3-yl)carbonyl]alanyl-L-valyl-*N*-1-~((1R,2Z)-4-(benzyloxy)-4-oxo-1-[(3R)-2-oxopyrrolidin-3-yl]methyl)but-2-enyl)-L-leucinamide (N3) were used as reference molecules against hACE-2 and M^{Pro} , respectively.

At first, water molecules were removed from the complex. Using the valence monitor method, the incorrect valence atoms were corrected. The energy minimization was then accomplished through the application of force fields CHARMM and MMFF94 [42–45]. The binding sites were defined and prepared for docking processes. Structures of the tested isoflavonoids and the co-crystallized ligands were sketched using ChemBioDraw Ultra 14.0 (PerkinElmer, Waltham, MA, USA) [46] and saved as MDL-SD files. Next, the MDL-SD files were opened, 3D structures were protonated, and energy was minimized by implementing force fields CHARMM and MMFF94, then adjusted for docking. CDOCKER protocol was used for docking studies using CHARMM-based molecular dynamics (MD) to dock the co-crystallized ligands into a receptor binding site [47,48]. In the docking studies, a total of 10 conformers were considered for each molecule. Finally, according to the minimum free energy of binding interaction, the most ideal pose was chosen.

The toxicity parameters for the examined compounds were calculated using *Discovery studio 4.0* software (Accelrys software Inc., San Diego, CA, USA). Simeprevir was used as a reference drug. At first, the CHARMM force field was applied then the compounds were prepared and minimized according to the preparation of small molecule protocol. Then different parameters were calculated from the toxicity prediction (extensible) protocol.

3. Results and Discussion

3.1. Pharmacokinetic Profiling Study

3.1.1. Lipinski's Rule of Five

In the present study, an *in silico* computational study of compounds (1–59) was performed to determine their physicochemical properties according to the directions of Lipinski's rule of five [38] (Table 1).

Table 1. physicochemical properties of the tested isoflavonoids.

Comp.	Lipinski's Rule of Five			
	Log P ^a	Molecular Weight	HBD ^b	HBA ^c
1	2.14	270.23	3	5
2	2.38	254.23	2	4
3	2.36	284.26	2	5
4	3.16	332.34	2	6
5	3.17	302.32	2	5
6	3.81	322.35	2	4
7	3.09	328.31	1	6
8	2.78	256.25	3	4
9	2.68	270.28	1	4
10	3.48	322.35	1	4
11	3.23	338.35	2	5
12	−1.50	450.41	1	10
13	2.12	300.26	3	6
14	2.57	328.31	1	6
15	2.10	330.28	3	7
16	2.33	344.31	2	7
17	2.55	358.34	1	7
18	2.34	314.28	2	6
19	2.60	326.3	0	6
20	2.61	296.27	0	5
21	2.36	284.26	2	5
22	2.34	314.28	2	6
23	2.58	356.32	0	7
24	2.10	330.28	3	7
25	2.36	284.26	2	5
26	2.59	298.2	1	5
27	4.84	358.38	2	4
28	6.04	420.49	2	5
29	6.07	420.49	2	5
30	5.03	436.49	3	6
31	5.03	436.49	3	6
32	3.95	418.43	2	6
33	4.78	420.45	3	6
34	3.68	438.4	4	7
35	3.73	436.45	4	7
36	2.90	354.35	4	6
37	5.61	422.4	4	6
38	3.9	368.38	3	6
39	1.91	288.25	4	6
40	2.14	302.27	3	6
41	2.46	316.3	2	6
42	2.44	346.33	2	7
43	2.465	316.3	2	6
44	2.24	302.27	3	6
45	2.48	332.3	4	7
46	1.99	318.278	4	7
47	1.88	302.27	3	6
48	4.11	340.37	3	5
49	4.09	370.39	3	6
50	4.09	370.39	3	6
51	4.32	384.422	2	6
52	4.32	384.42	2	6
53	6.19	422.51	2	5
54	6.19	422.51	2	5
55	4.32	384.42	2	6
56	5.72	424.48	4	6
57	6.21	392.48	2	4
58	4.52	452.49	3	7
59	5.95	438.51	3	6

^a Partition coefficient; ^b Hydrogen bond donors; ^c Hydrogen bond acceptors.

It was found that almost all the tested isoflavonoids followed Lipinski's rule of five and hence display a drug-like molecular (DLM) nature. The Log P, molecular weight, number of H-bond donors and number of H-bond acceptors of all isoflavonoids are within

the accepted values (less than 5, 500, 5 and 10, respectively). with exceptions of compounds (28, 29, 53, 54 and 57) that have log p values of 6.04, 6.07, 6.19, 6.19 and 6.21, respectively.

3.1.2. ADMET Studies

Discovery studio 4.0 software was used to predict ADMET descriptors (absorption, distribution, metabolism, excretion and toxicity) for the selected isoflavonoids using remdesivir as a reference drug. The predicted ADMET parameters of the tested compounds were listed in Table 2. The BBB penetration levels of 6, 10 and 27 were expected to be high. On the other hand, the expected BBB penetration levels of all other isoflavonoids were ranging from medium to low. These results indicate that most of the tested compounds would be less likely to penetrate the CNS.

Table 2. Predicted ADMET descriptors for the tested isoflavonoids and remdesivir.

Compound	BBB Level ^a	Absorption Level ^b	PPB ^c	Solubility Level ^d
1	3	0	2	3
2	2	0	2	3
3	3	0	1	3
4	2	0	0	3
5	2	0	2	3
6	1	0	0	2
7	2	0	0	2
8	2	0	1	3
9	2	0	2	3
10	1	0	2	2
11	2	0	0	2
12	4	2	0	4
13	3	0	1	3
14	3	0	2	3
15	3	0	2	3
16	3	0	1	3
17	3	0	1	3
18	3	0	2	3
19	2	0	2	2
20	2	0	1	2
21	3	0	1	3
22	3	0	1	3
23	2	0	2	2
24	3	0	2	3
25	3	0	2	3
26	2	0	2	3
27	1	0	2	2
28	4	1	2	2
29	4	1	2	1
30	4	1	2	2
31	4	1	2	2
32	2	0	0	2
33	4	1	1	2
34	4	1	0	2
35	4	1	0	2
36	4	0	1	3
37	4	2	2	2
38	4	0	0	2
39	3	0	1	3
40	3	0	1	3
41	3	0	2	3
42	3	0	2	3
43	3	0	0	3
44	3	0	2	3

Table 2. Cont.

Compound	BBB Level ^a	Absorption Level ^b	PPB ^c	Solubility Level ^d
45	4	0	2	3
46	4	0	0	3
47	3	0	0	3
48	2	0	1	2
49	4	0	2	2
50	4	0	1	2
51	2	0	1	2
52	2	0	2	2
53	4	2	2	1
54	4	2	2	1
55	2	0	1	2
56	4	2	2	2
57	4	1	2	1
58	4	1	1	2
59		2	2	2
Remdesivir	4	3	0	2

^a BBB level, blood brain barrier level, 0 = very high, 1 = high, 2 = medium, 3 = low, 4 = very low. ^b Absorption level, 0 = good, 1 = moderate, 2 = poor, 3 = very poor. ^c PPB, plasma protein binding, 0 means less than 90%, 1 means more than 90%, 2 means more than 95%. ^d solubility level, 0 = extremely low, 1 = very low, 2 = low, 3 = good, 4 = optimal.

The plasma protein binding model predicts the binding ability of a ligand with plasma proteins which affects its efficiency. The results revealed that compounds **1, 2, 5, 9, 10, 14, 15, 18, 19, 23–31, 37, 41, 42, 44, 45, 49, 52–54, 56, 57** and **59** were expected to bind plasma protein by more than 95%, while **3, 8, 13, 16, 17, 20–22, 33, 39, 40, 48, 50, 51, 55** and **58** showed a binding pattern of more than 90%. Contrastingly, compounds **4, 6, 7, 11, 12, 32, 34, 35, 38, 43, 46** and **47** were expected to bind the plasma protein less than 90%.

Moreover, all the tested isoflavonoids were predicted to have good absorption behavior better than that of remdesivir. Also, the solubility levels of most compounds were expected to be in the good range (Table 2 and Figure 2).

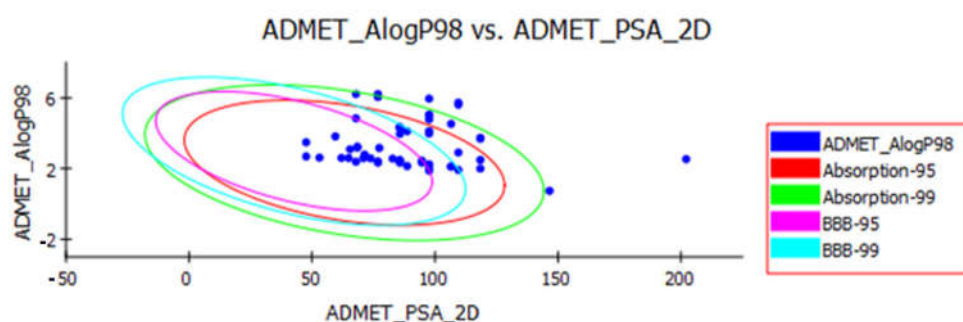


Figure 2. The expected ADMET study of the designed compounds and remdesivir.

3.2. Molecular Docking

3.2.1. Validation Process

Validation of the docking procedures was achieved via re-docking of the co-crystallized ligands against the active pocket of hACE2 and M^Pro. The calculated RMSD values between the re-docked poses and the co-crystallized ones were 2.4 and 2.8 Å. Such values of RMSD indicated the efficiency and validity of the docking processes (Figure 3).

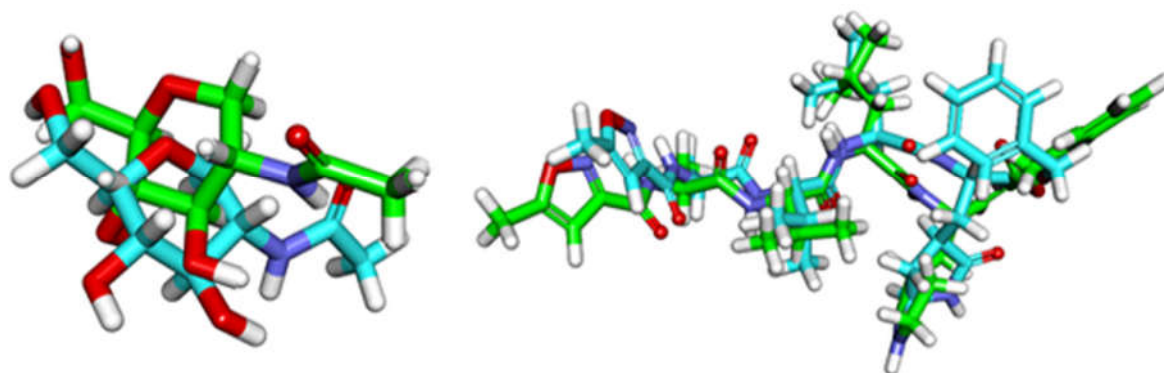


Figure 3. Superimposition of the co-crystallized poses (green) and the docking pose (maroon) of the same ligands. **(Left):** hACE2 (RMSD = 2.4 Å), **(right):** M^{Pro} (RMSD = 2.8 Å).

3.2.2. HACE2

Coronavirus spike receptor-binding domain complexed with its receptor hACE-2 (PDB: 6LZG) used as a target for the docking studies of selected isoflavonoids. The results demonstrated that all isoflavonoids bound strongly to hACE-2 with binding energies better than that of the co-crystallized ligand (NAG). This indicated that the affinity of the tested isoflavonoids toward hACE-2 is higher than that of the co-crystallized ligand (Table 3). Moreover, almost all the tested isoflavonoids exhibited binding modes similar to that of NAG.

Table 3. Free binding energies of the selected isoflavonoids and the co-crystallized ligand (NAG) against hACE-2 and amino acid residues involved in H. bonds and hydrophobic interaction.

Comp.	Binding Energy (kcal mol ⁻¹)	No. of H. Bonds	Involved Amino Acid Residues	Amino Acid Residues Involved in Hydrophobic Interaction
1	-30.90	2	Ser371, Asn343	Phe374, Gly339, Ser371, Phe338, Phe342
2	-27.84	1	Ser371	Phe338, Phe342, Gly339
3	-28.13	1	Ser371	Phe374, Phe342, Phe338, Gly339
4	-25.52	1	Ser371	Phe374, Phe342, Phe338, Gly339
5	-24.12	1	Ser371	Phe374, Phe342, Phe338, Leu368, Gly339
6	-26.14	1	Ser371	Phe342, Phe338, Phe374
7	-25.95	1	Ser371	Phe342, Phe338, Phe374
8	-27.41	2	Ser371, Asn343	Phe374, Phe342, Phe338
9	-22.32	1	Ser371	Phe374, Phe342, Phe338
10	-23.66	0	0	Phe374, Phe342, Phe338, Ser371, Gly339
11	-24.02	1	Ser371	Phe374, Phe342, Phe338
12	-31.01	2	Asp364	Phe338, Ser371, Leu368, Cys336, Phe374, Val367
13	-27.85	0	0	Asn343, Ser371, Leu368, Cys336, Phe374, Val367
14	-25.17	1	Cys336	Phe338, Ser371, Ser373, Leu368, Cys336, Phe374, Val367
15	-27.52	1	Cys336	Phe374, Phe342, Ser371, Leu368, Cys336, Val367
16	-27.42	1	Cys336	Ser371, Leu368, Cys336, Phe374, Val367, Gly339
17	-25.02	1	Trp436	Phe374, Leu368, Val367, Phe342
18	-23.37	1	Cys336	Phe338, Leu368, Cys336, Phe342, Val367, Asn343
19	-30.52	1	Gly339	Phe374, Phe338, Ser371, Gly339, Cys336, Leu368, Val367
20	-29.50	0	0	Phe374, Phe338, Ser371, Cys336, Leu368, Val367
21	-24.10	0	0	Phe338, Ser371, Cys336, Leu368, Val367, Phe374
22	-28.66	1	Cys336	Asn434, Phe338, Ser371, Cys336, Leu368, Val367
23	-33.20	0	0	Phe338, Ser371, Cys336, Leu368, Val367, Ser373
24	-32.74	2	Ser371, Cys336	Phe374, Phe338, Gly339, Cys336, Ser371, Leu368, Phe432

Table 3. Cont.

Comp.	Binding Energy (kcal mol ⁻¹)	No. of H. Bonds	Involved Amino Acid Residues	Amino Acid Residues Involved in Hydrophobic Interaction
25	-24.43	1	Ser373	Gly339, Leu368, Phe338, Ser371, Cys336
26	-27.27	1	Ser373	Asn343, Gly339, Leu368, Phe338, Ser371, Cys336
27	-30.81	1	Cys336	Phe374, Phe338, Ser371, Cys336, Leu368, Val367, Phe342, Asn343
28	-29.91	0	0	Leu368, Val367, Phe342, Asn343, Cys336, Phe338, Ser371,
29	-32.76	2	Ser371, Cys336	Phe374, Phe338, Ser371, Val367, Cys336, Leu368, Ser373
30	-29.12	2	Asn343, Cys336	Phe338, Ser371, Gly339, Cys336, Leu368, Ser373, Asn343
31	-30.84	1	Asn364	Cys336, Leu368, Ser373, Asn343, Val362, Asn364
32	-33.95	0	0	Phe338, Val367, Cys336, Leu368, Ser373, Asn440, Asn364
33	-36.35	1	Ser371	Phe374, Phe342, Ser371, Asn343, Cys336, Glu340, Ser373
34	-39.33	1	Asp364	Phe338, Phe342, Asn343, Val367, Asp364, Cys336, Leu335, Leu386
35	-34.48	3	Cys336, Gly339, Glu340	Phe374, Phe338, Val367, Cys336, Leu368, Ser373, Gly339, Glu340
36	-34.80	2	Cys336, Gly339	Phe338, Leu335, Asn343, Ser373
37	-34.37	2	Ser371, Ser373	Leu368, Ser371, Asn343, Ser373, Phe338, Phe342
38	-30.09	2	Cys336, Gly339	Phe338, Leu335, Cys336, Gly339, Asn343, Ser373
39	-25.26	1	Ser371	Phe374, Phe338, Ser371, Val367, Cys336, Leu368, Ser373
40	-23.32	1	Ser373	Phe338, Val367, Cys336, Leu368, Ser373
41	-29.16	1	Cys336	Cys336, Phe338, Val367, Leu368, Ser373
42	-32.12	1	Ser371	Phe374, Val367, Cys336, Leu368, Ser373, Phe338, Ser371,
43	-27.79	1	Ser371	Phe374, Phe338, Ser371, Val367, Cys336, Leu368
44	-27.53	1	Ser373	Phe338, Phe374, Val367, Cys336, Leu368, Ser373
45	-31.39	1	Cys336	Cys336, Phe342, Val367, Leu368, Gly339, Asp364
46	-30.09	2	Cys336, Gly339	Phe338, Leu335, Cys336, Gly339, Asn343, Ser373
47	-25.11	0	0	Phe338, Asn343, Cys336, Leu368, Ser373
48	-34.79	1	Cys336	Cys336, Asn343, Phe338, Val367, Leu368, Ser373
49	-31.79	1	Cys336	Phe338, Asn343, Cys336, Leu368, Val367
50	-30.39	1	Cys336	Cys336, Phe338, Val367, Leu368, Ser373
51	-30.81	1	Ser371	Phe342, Asn343, Phe374, Ser371, Leu368
52	-29.33	1	Gly339	Phe338, Leu335, Cys336, Gly339, Val367, Asn343, Ser373
53	-33.34	1	Ser373	Phe338, Phe374, Val367, Cys336, Leu368, Ser373
54	-35.10	0	0	Ser371, Ser373, Phe338, Leu335, Cys336
55	-29.06	1	Cys336	Cys336, Phe342, Val367, Leu335, Ser371, Asn343
56	-34.90	2	Ser371, Cys336	Phe374, Phe338, Ser371, Val367, Cys336, Leu368, Ser373
57	-34.77	0	0	Ser373, Phe338, Phe342, Cys336, Gly339
58	-30.22	1	Ser371	Phe342, Asn343, Phe374, Ser371, Leu368
59	-34.70	1	Ser371	Ser373, Asn343, Phe374, Ser371, Leu368, Val367, Leu335
NAG	-21.39	1	Ser371.	Phe374, Phe342, Phe338

The binding pattern of co-crystallized ligand (NAG) demonstrated single hydrogen bonding interaction with Ser371 residue (Figure 4). NAG showed binding energies of

−21.39 kcal mol^{−1}. It was found that most of the tested isoflavonoids exhibited binding modes similar to the reference molecule. Compounds **1** (−30.90 kcal mol^{−1}) and **8** (−27.41 kcal mol^{−1}) demonstrated an additional hydrogen bond with Asn343 residue (Figures 5 and 6). This extra hydrogen bond may account for the relatively high binding affinity of both compounds. Furthermore, compounds **33** (Figure 7) and **56** (Figure 8) were found to have good binding energy values of −36.35 and −34.90 kcal mol^{−1}, respectively. Compound **33** formed a binding mode like that of the reference ligand as it formed one hydrogen bond with Ser371 and seven hydrophobic interactions with Phe374, Phe342, Ser371, Asn343, Cys336, Glu340, and Ser373. Interestingly, compound **56** formed two hydrogen bonds with Ser371 and Cys336 in addition to seven hydrophobic interactions with Phe374, Phe338, Ser371, Val367, Cys336, Leu368, and Ser373.

Such results indicate the significance of the tested isoflavonoids as potential inhibitors for hACE-2. Consequently, such compounds may inhibit the entrance of coronavirus into human cells.

3.2.3. Main Protease (M^{Pro})

The docking results of isoflavonoids into the active site of coronavirus M^{Pro} (PDB: 6LU7) were listed in Table 4. The results showed that all tested isoflavonoids can bind to M^{Pro} with one or more hydrogen bonds. At the same time, the tested compounds bound to the receptor with free binding energies ranging from −32.19 to −50.79 kcal mol^{−1}, compared to the co-crystallized (binding energy = −62.84 kcal mol^{−1}).

These results revealed that the affinities of the presented isoflavonoids against M^{Pro} are lower than that of N3. Despite that, the binding energies are still considerable, and their binding modes are great which making these isoflavonoids seem to be biologically active ligands to some extent. Figures 9–14 illustrate the binding patterns of N3, compound **6** (binding energy = −41.41 kcal mol^{−1}), compound **7** (binding energy = −40.11 kcal mol^{−1}), compound **8** (binding energy = −42.73 kcal mol^{−1}), compound **30** (binding energy = −48.39 kcal mol^{−1}), and compound **53** (binding energy = −46.90 kcal mol^{−1}), respectively.

Compound **30** formed a binding mode like that of the reference ligand as it formed three hydrogen bonds with Glu166, Tyr54, and Asp187. Furthermore, it formed eight hydrophobic interactions with His41, Gln189, His163, Met165, Tyr54, Asp187, Leu167, and Glu166. For compound **53**, it formed two hydrogen bonds with Glu166, Phe140. Besides, it formed six hydrophobic interactions with Glu166, Gln189, Leu141, Met165, His172, and Phe140.

Table 4. Free binding energies of studied isoflavonoids and ligand to coronavirus M^{Pro} and amino acid residues involved in H. bonds and hydrophobic interaction.

Comp.	Binding Energy (kcal mol ^{−1})	No. of H. Bonds	Involved Amino Acid Residues	Amino Acid Residues Involved in Hydrophobic Interaction
1	−37.38	1	Glu166	Phe140, Leu141, Gln189, His41, Tyr54, Glu166
2	−35.91	1	Phe140	Phe140, Leu141, Gln189, His41, Tyr54, Glu166
3	−36.08	1	Glu166	Phe140, Leu141, Gln189, His41, Tyr54, Glu166
4	−37.99	1	Glu166	Phe140, Leu141, Gln189, His41, Tyr54, Glu166
5	−38.45	2	Thr190, Leu141	Phe140, Leu141, Gln189, His41, Tyr54, Glu166
6	−41.41	1	Glu166	Phe140, Leu141, Asn142, His163, Tyr54, Glu166
7	−40.11	1	Glu166	Phe140, His172, Glu166, His163, His164, Gln189
8	−42.73	3	Glu166, Cys145, His163	Phe140, Leu141, Glu166, His163, His164, Gln189
9	−33.98	1	Phe140.	Phe140, Leu141, Gln189, His41, Tyr54, Glu166
10	−35.25	2	Glu166, Phe140.	Phe140, Leu141, Gln189, His41, Tyr54, Glu166
11	−32.19	1	Glu 166	Phe140, Leu141, Gln189, His41, Tyr54, Glu166
12	−41.55	3	Gln192, His41, Arg188	Glu166, Met 165, Gln192, His41, His164, His172
13	−40.51	1	Glu 166	Met 165, Cys145, His41, Asn142, Glu166
14	−39.89	1	Glu 166	His163, Met 165, Cys145, His41, Glu189, Glu166
15	−37.34	1	Glu166	Phe140, Met 165, Asp187, His41, Glu189, Glu166
16	−39.05	6	Glu166, Cys145, Thr26	Glu166, Cys145, Thr26, His41, Met 165, Glu189, Leu27

Table 4. Cont.

Comp.	Binding Energy (kcal mol ⁻¹)	No. of H. Bonds	Involved Amino Acid Residues	Amino Acid Residues Involved in Hydrophobic Interaction
17	-40.60	1	Gly143	Glu166, Cys145, Thr26, His4, Met 165, Gln189, Gln192
18	-35.58	0	0	Glu166, Phe140, Gly143, Asp187, Met 165, Gln189
19	-37.26	0	0	Glu166, Phe140, Cys145, Asp142, Met 165, Gln189
20	-34.97	1	Glu 166	Phe140, Gln189, His41, Ser144, Tyr54, Glu166
21	-38.42	1	Phe140	Phe140, Leu141, Gln189, His41, Met165, Leu140, Glu166
22	-40.14	1	Phe140	Phe140, Leu141, Gln189, His164, Met165, Leu140, Glu166
23	-40.24	0	0	Glu166, Phe140, Leu141, Gln189, His41, Met165, Leu140
24	-38.90	2	Phe140, Glu166	Glu166, Phe140, Leu141, Gln189, His164, Met165, Leu140, Cys145
25	-34.43	2	Phe140, Glu166	Glu166, Phe140, His41, Gln189, His164, Met165, Cys145
26	-36.39	1	Phe140	Glu166, Phe140, His41, Gln189, His164, Met165
27	-38.58	3	Gly143, Cys145, Thr26	Glu166, Gly143, Gln189, Cys145, Thr26, Met165
28	-47.62	1	His41	Glu166, Phe140, His41, Gln189, His164, Met165, Cys145, Leu141
29	-49.64	3	Glu166, Tyr54, Asp187	Phe140, Gln189, His172, Met165, Tyr54, Asp187, Leu167, Glu166
30	-48.39	3	Glu166, Tyr54, Asp187	His41, Gln189, His163, Met165, Tyr54, Asp187, Leu167, Glu166
31	-48.32	1	Glu 166	Phe140, Gln189, His41, Met165, Tyr54, Glu166
32	-38.31	1	Cys145	Gln189, His41, Met165, Cys145, Glu166
33	-43.52	2	Gln189, Gly143	Met165, Gln189, Gly143, Glu166
34	-45.48	2	Glu166, Cys145	Glu166, Phe140, His41, Gln189, His164, Met165, Cys145
35	-41.38	1	Gly143	Glu166, Gly143, Leu107, Gln192, His164, Met165, Cys145
36	-42.29	4	His164, Cys145, Ser144, Leu141	Gln189, His172, Met165, Glu166 His164, Cys145, Ser144, Leu141
37	-48.13	4	Met165, Thr190, His41, Cys145	Glu166, Met165, Thr190, His41, Cys145, Gln189
38	-43.30	1	Glu 166	Gln189, His163, Met165, Ser144, Glu166, Leu167
39	-38.05	4	Glu166, Cys145	Glu166, Cys145, Met165, Asn142
40	-36.12	2	Glu166, His163	Glu166, His163, Phe140, Met165
41	-38.22	3	Gln189, Asp187, Tyr54	Gln189, Met165, His163, Glu166
42	-37.17	1	Glu166	Glu166, Leu141, Gln189, Gly143
43	-35.41	1	Asp187	Glu166, Leu141, Met165, Ser144
44	-36.62	1	Glu166	Gln189, Met165, His172, Glu166, His163
45	-40.48	4	Ser144, Cys145, Thr26, Gly143	Cys145, Thr26, His163, Met165, Asn142
46	-40.84	1	His163	Glu166, His163, Phe140, Met165
47	-35.39	1	Glu166	Glu166, Asn142, His164, Met165
48	-40.40	1	His163	Glu166, Leu141, Met165, Gln189
49	-43.83	4	Glu166, Cys145, His41	Glu166, Cys145, His41, Met165, Asn142, Leu141
50	-43.91	1	Glu166	Glu166, Leu141, Met165, Gln189
51	-46.15	2	Glu166	Glu166, Ser144, Gln189, His41
52	-41.20	1	Glu166	Glu166, Leu141, Met165, Gln189, Asn142
53	-46.90	2	Glu166, Phe140	Glu166, Gln189, Leu141, Met165, His172, Phe140
54	-50.79	1	Glu166	Glu166, Gln189, Leu141, Met165, His172
55	-40.56	1	Thr26	Asn142, Glu166, Asn142, Leu141
56	-48.29	3	Glu166, His41	Glu166, His41, Met165, Asn142, His164
57	-49.89	2	Gly143, Arg188	Glu166, Gln189, Leu141, Met165, His163
58	-42.63	2	Glu166, Leu141	Glu166, Gln189, Leu141, Met165, His172
59	-48.11	2	Gly143, Leu141	Glu166, Gln189, Met165,
N3(Co-crystallized ligand)	-62.84	4	Gln189, Tyr54, Asp142, Asp187.	Phe140, Glu166, His172, Thr190, Gln189, Tyr54, Asp142, Asp187.

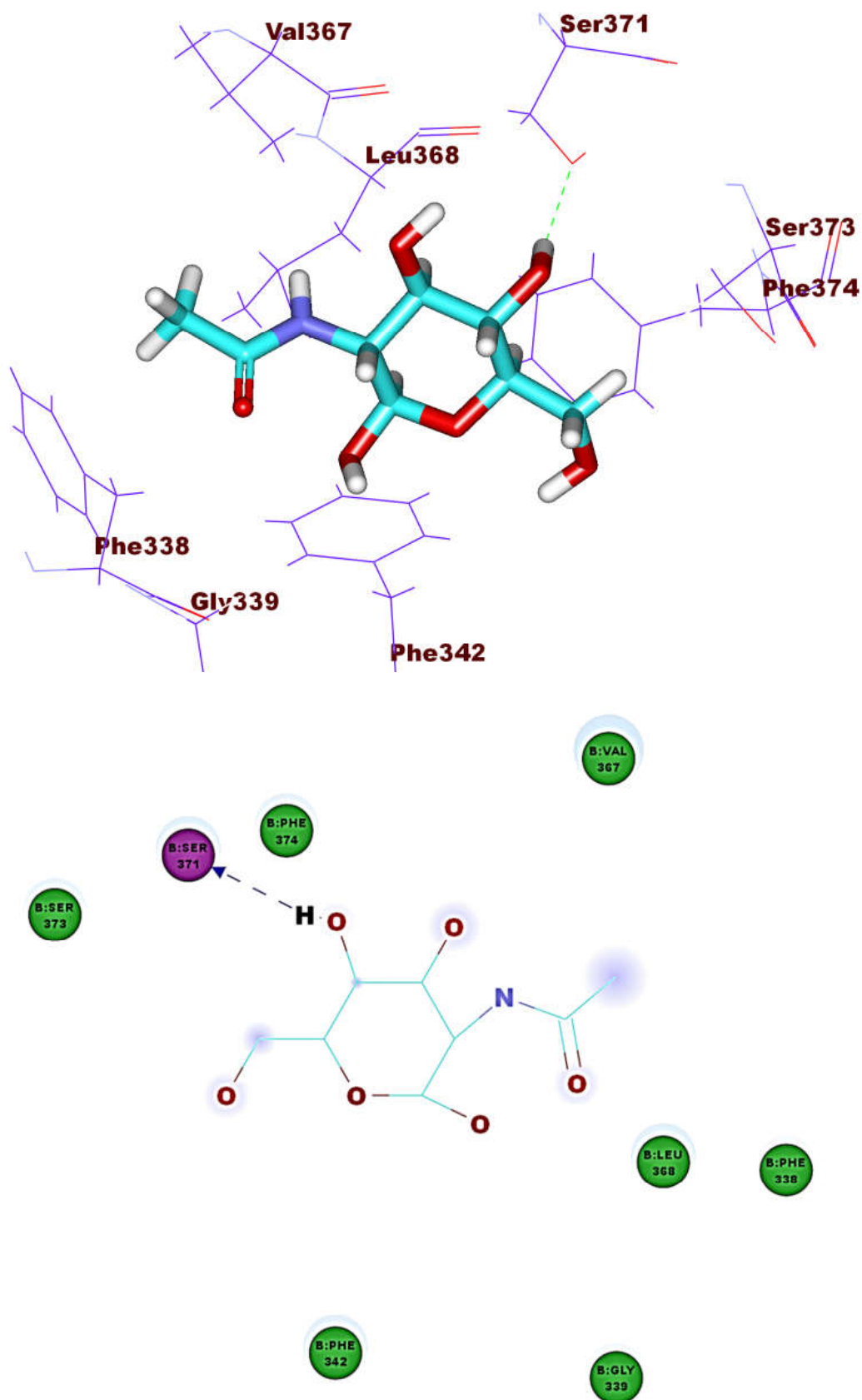


Figure 4. The co-crystallized ligand (NAG) docked into ACE-2, forming one H. bond with Ser371.

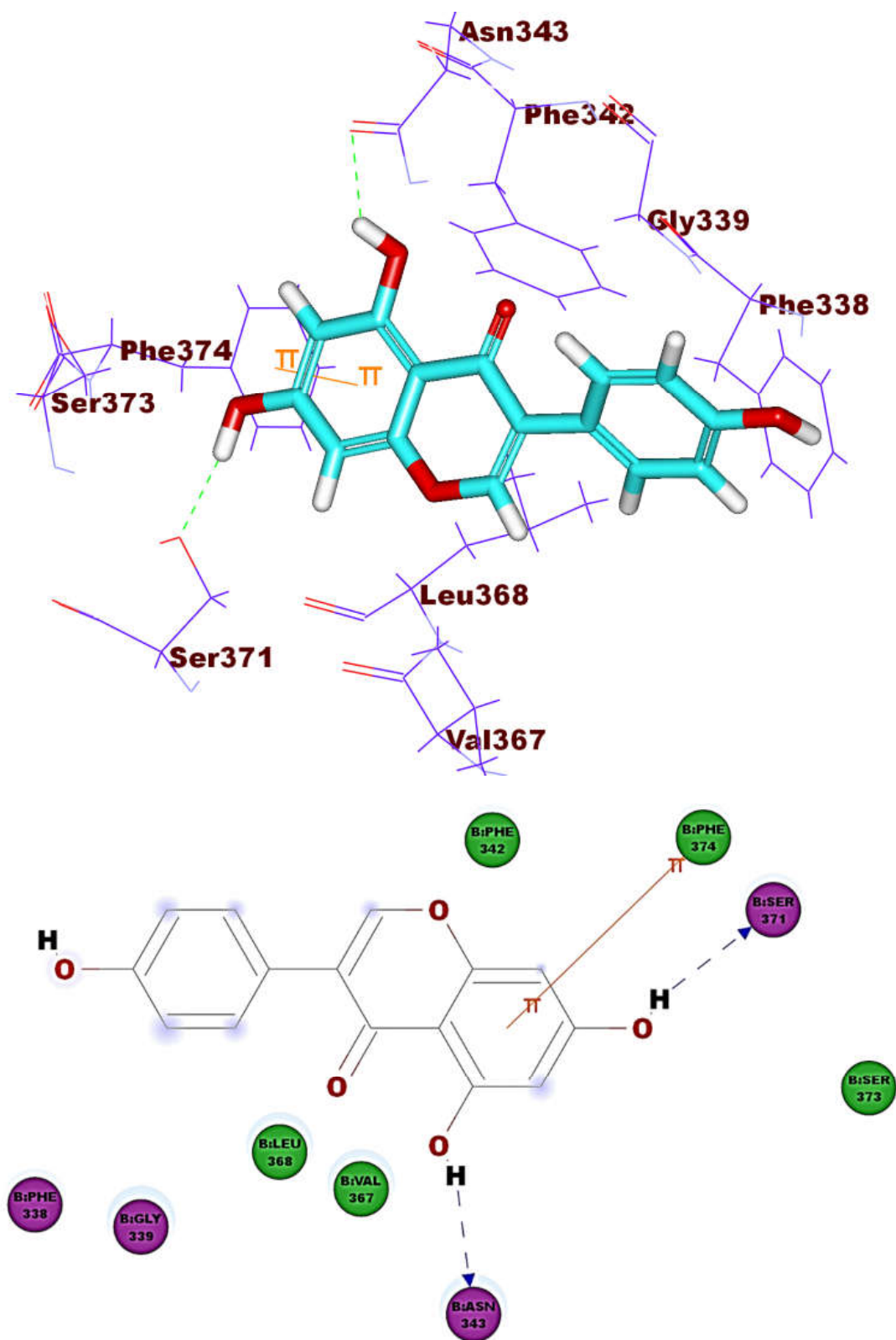


Figure 5. Compound 1 docked into ACE-2, forming two H. bonds with Ser371 and Asn343.

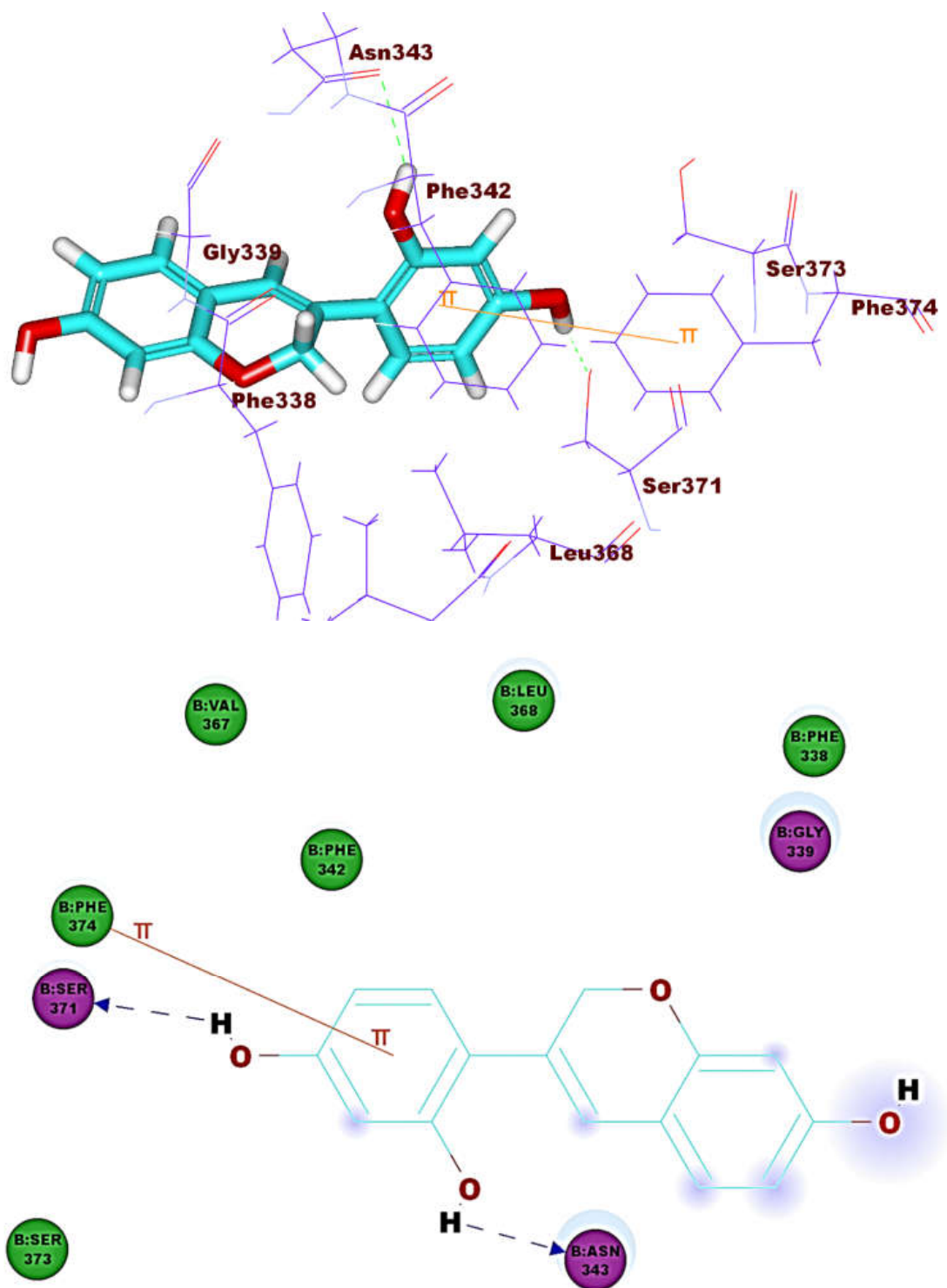


Figure 6. Compound 8 docked into ACE-2, forming two H. bonds with Ser371 and Asn343.

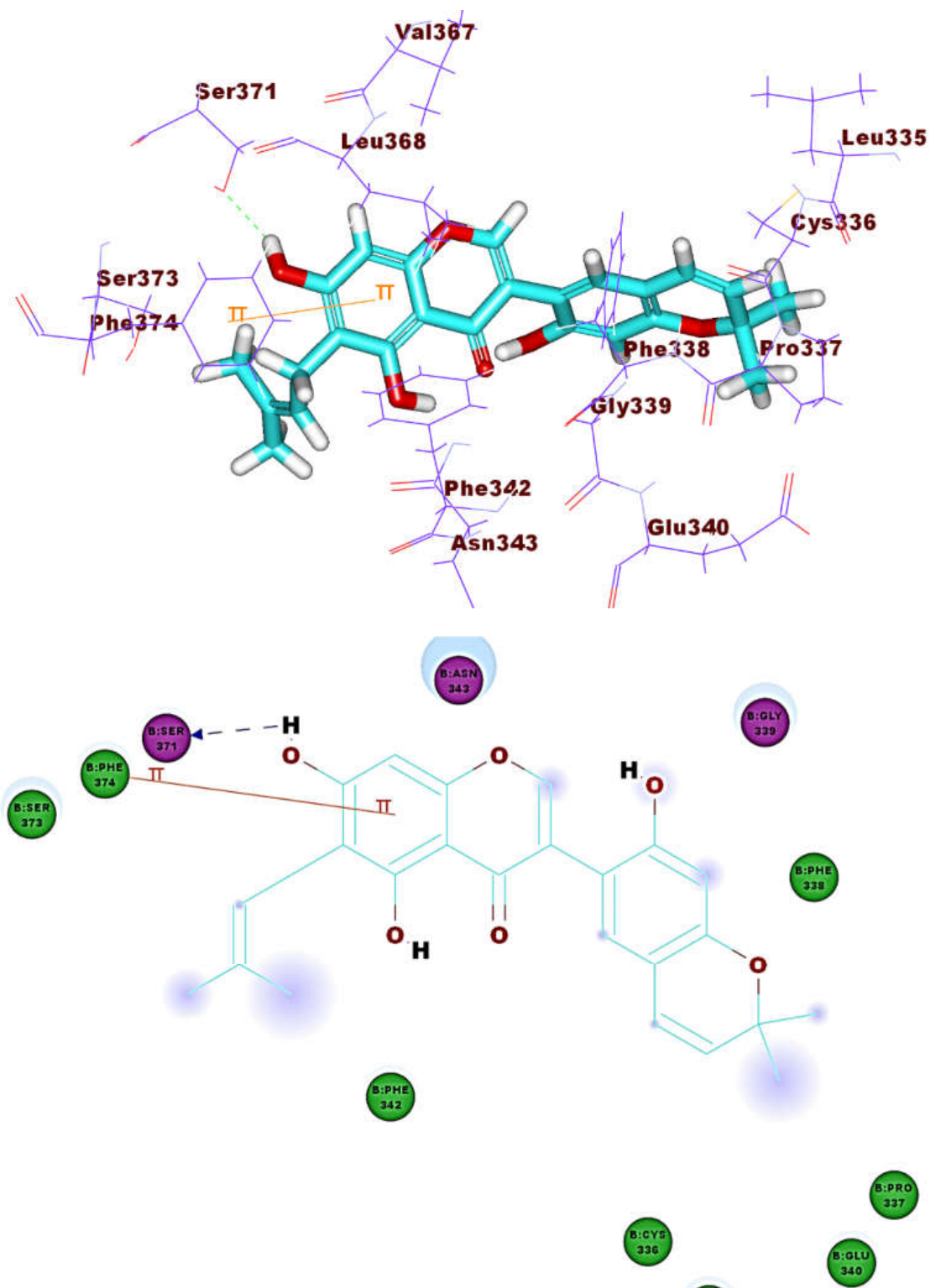


Figure 7. Compound 33 docked into ACE-2, forming one H. bond with Ser371.

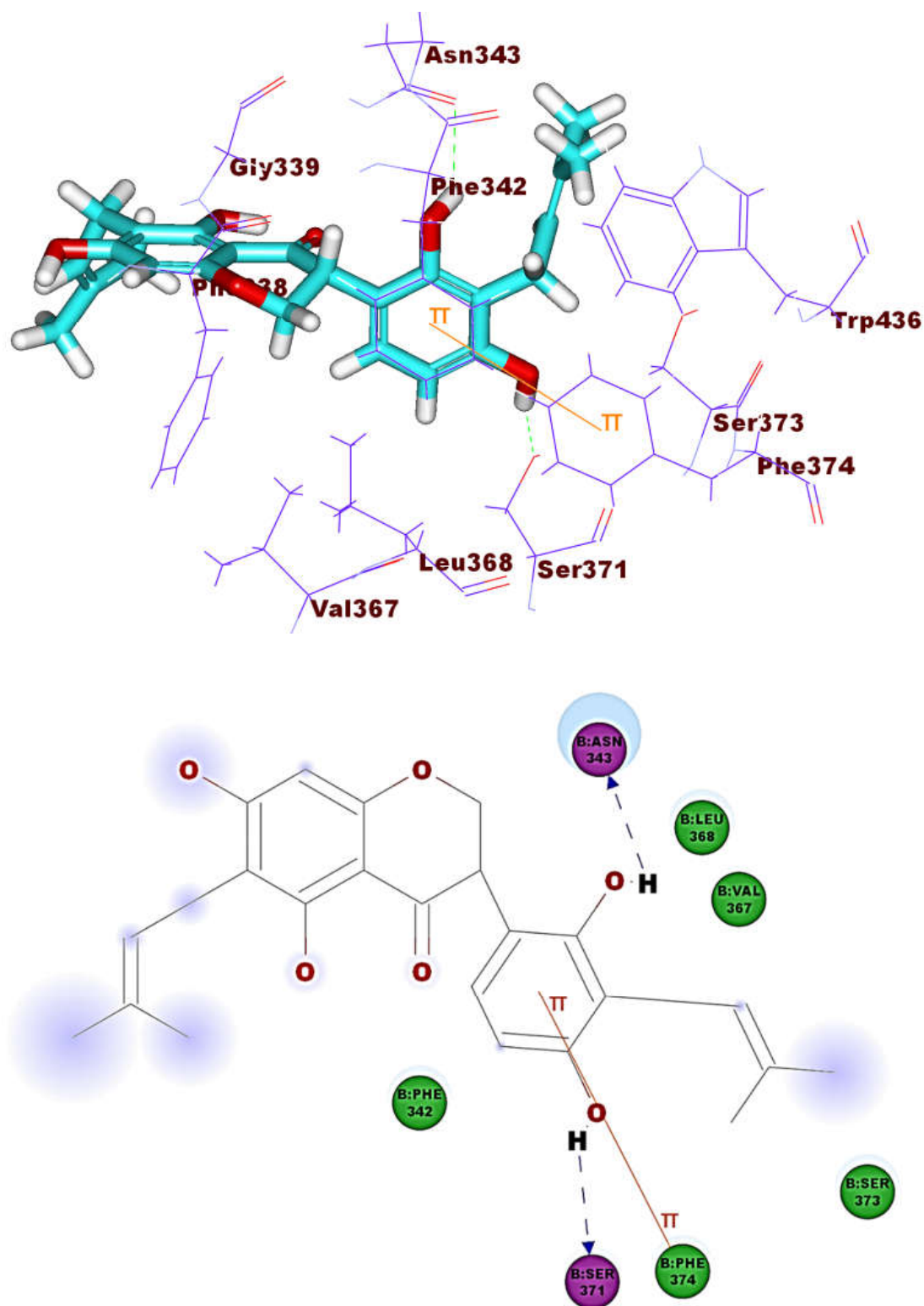


Figure 8. Compound 56 docked into ACE-2, forming two H. bonds with Ser371 and Cys336.

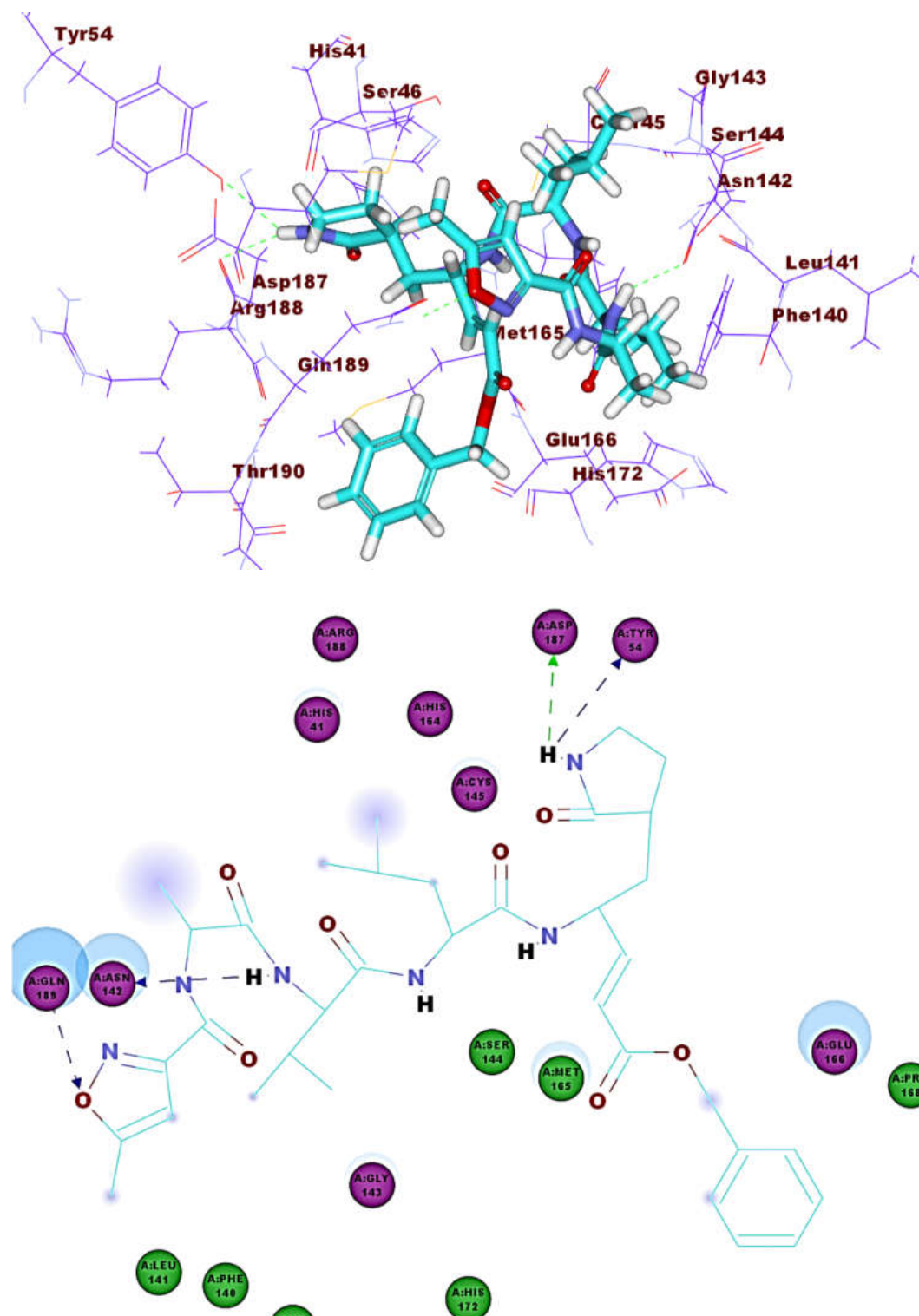
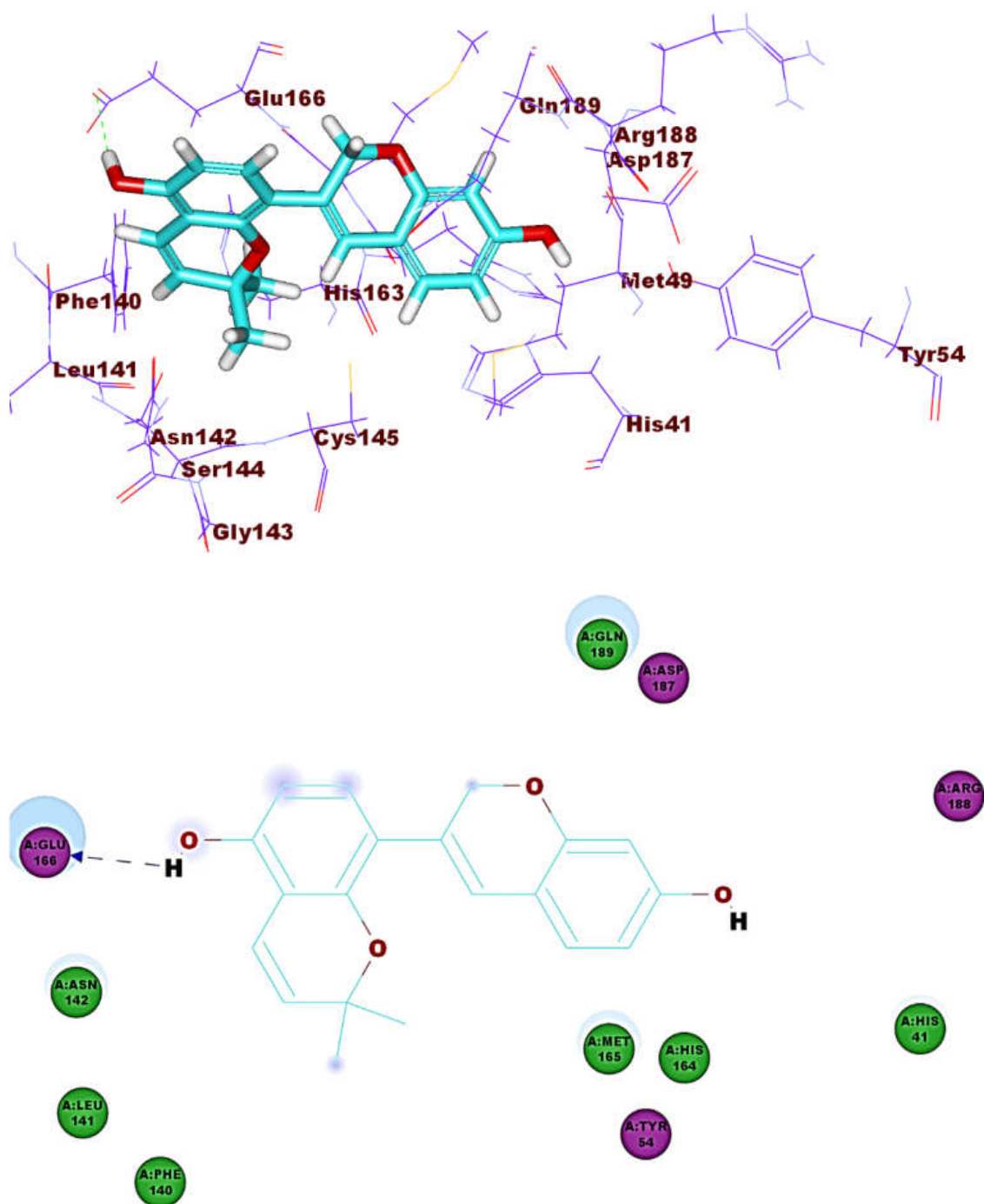


Figure 9. The co-crystallized ligand (N3) docked into M^{Pro}, forming four H. bonds with Gln189, Tyr 54, Asp 142, Asp187.



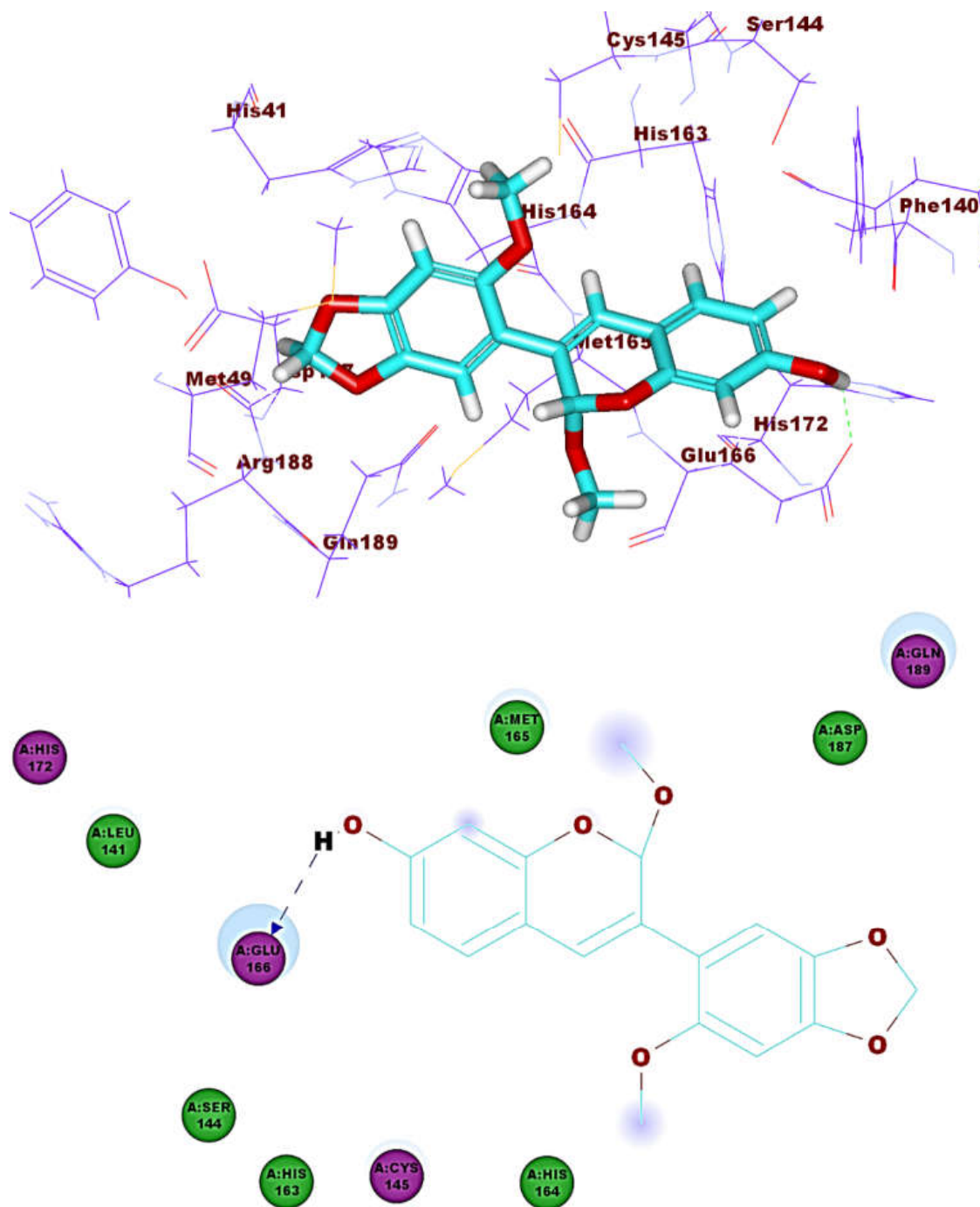


Figure 11. Compound 7 docked into MPro, forming one H. bond with Glu166.

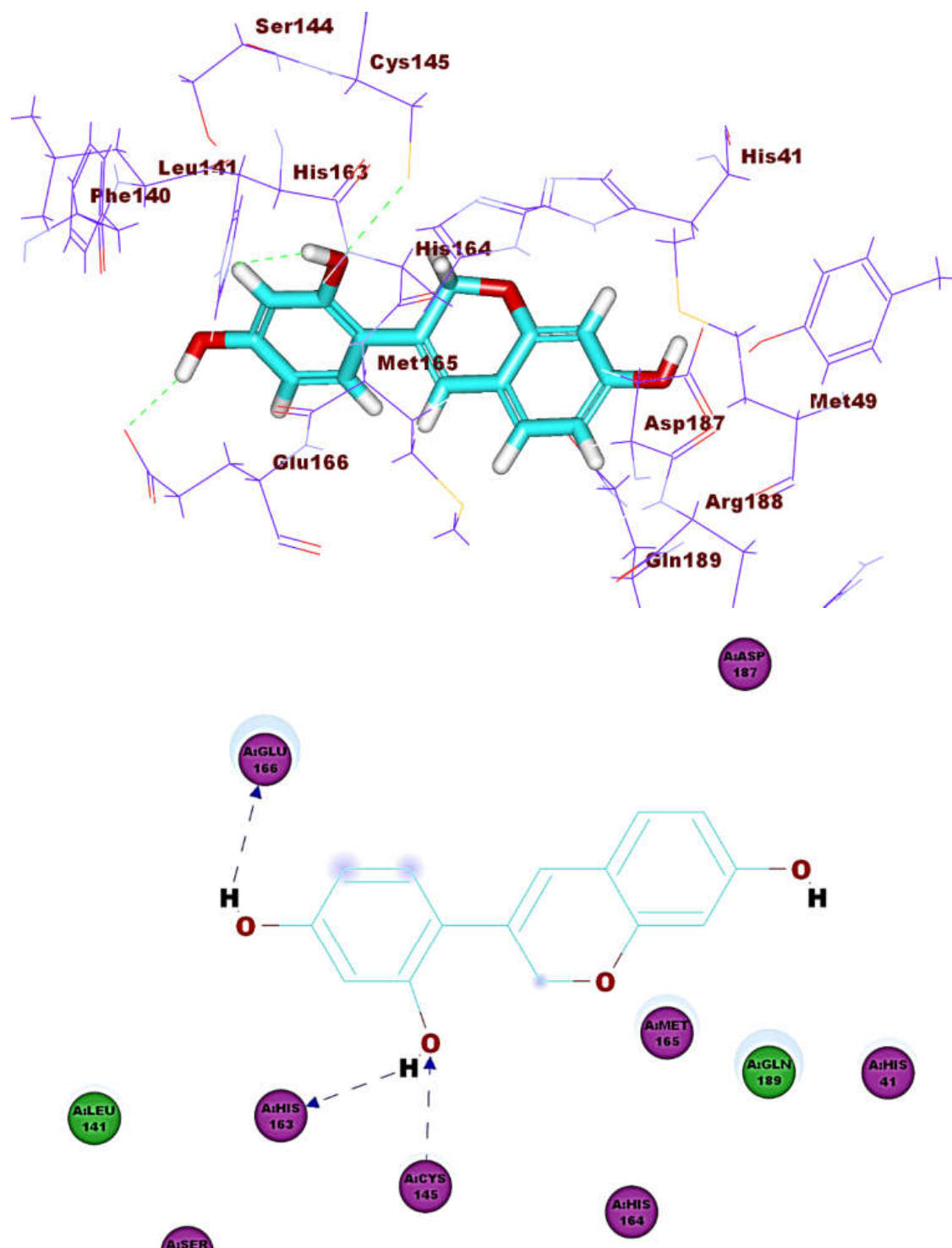


Figure 12. Compound 8 docked into M^{Pro}, forming three H. bonds with Glu166, Cys145 and His163.

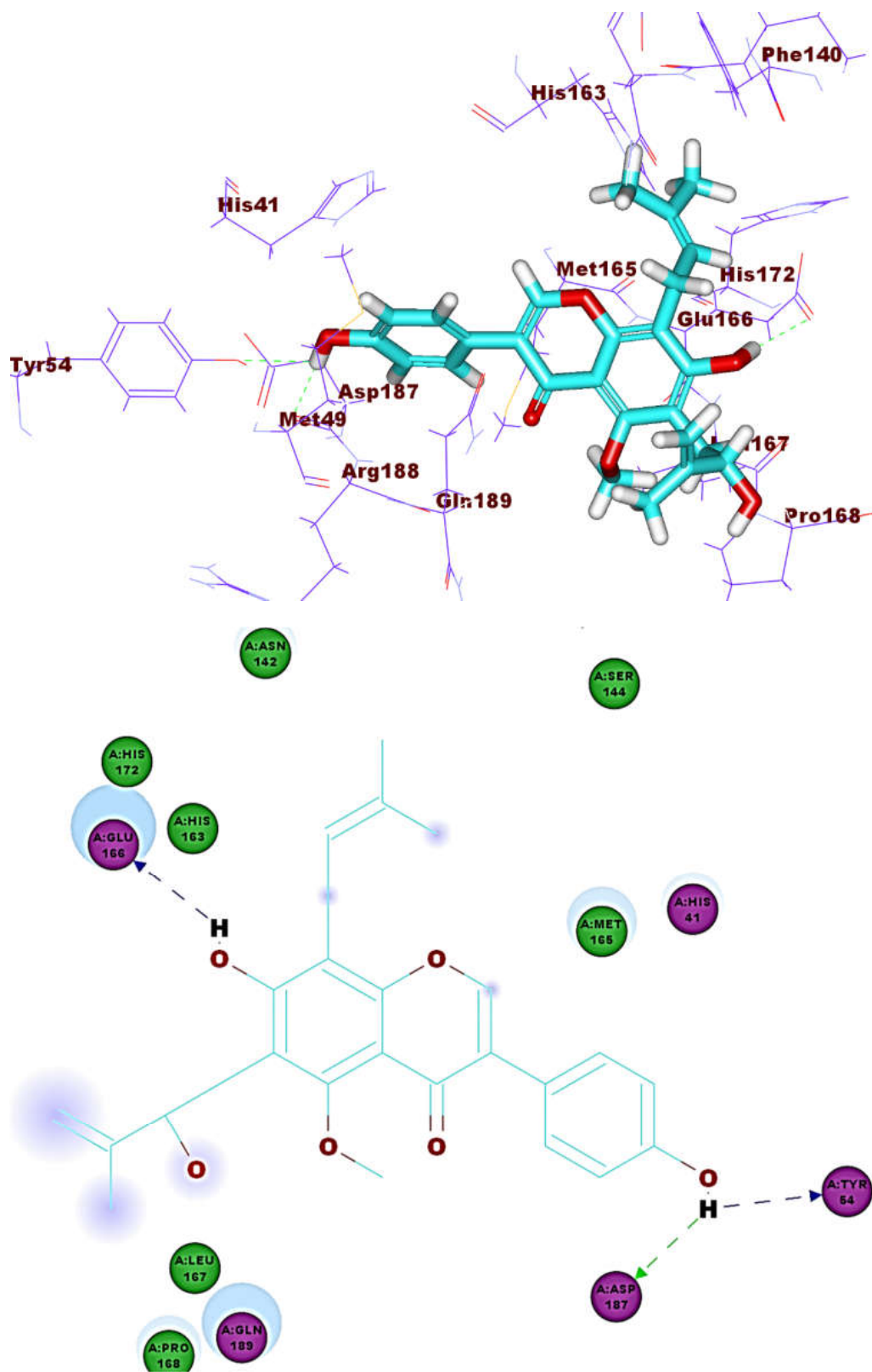


Figure 13. Compound 30 docked into M^{Pro}, forming three H. bonds with Glu166, Cys145 and His163.

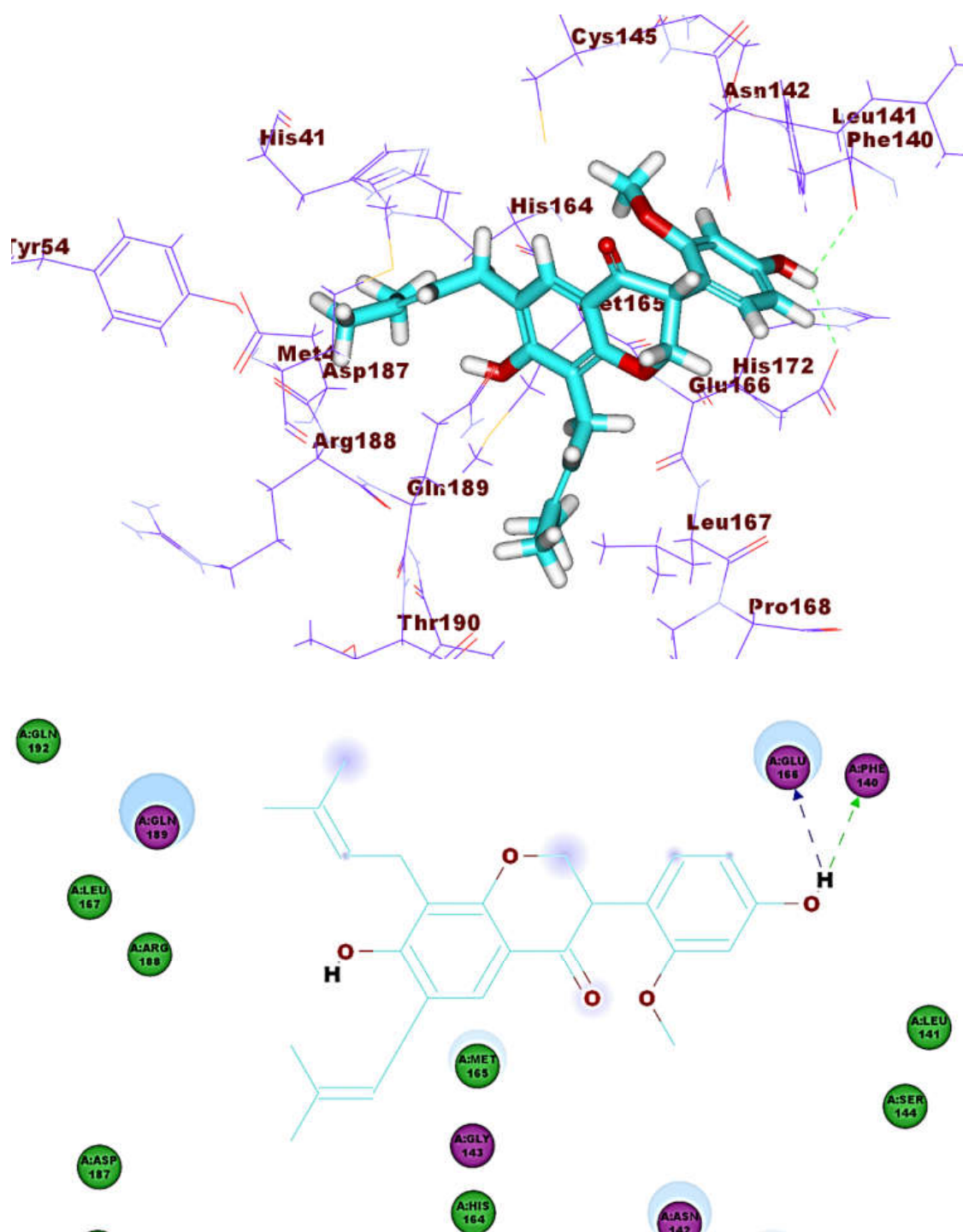


Figure 14. Compound 53 docked into M^{Pro} , forming two H. bonds with Glu166, Phe140.

3.2.4. Structure-Activity Relationship (SAR)

Based on the binding affinities of the tested compounds against hACE-2, we can obtain valuable SAR. Generally, the tested compounds showed decreased affinity against hACE-2 in descending order of isoflavone derivatives (compounds 34, 33, 35 and 37) > isoflavane derivatives (compounds 50, 53, 57 and 59) > isoflavone derivatives (compounds 19, 20 and 23) > isoflavone derivatives (compounds 1–3) > isoflava-3-ene derivatives (compounds

6–8) > isoflavane derivatives (compounds 4 & 5) > pterocarpanes derivatives (compounds 9–11) (Figure 15).

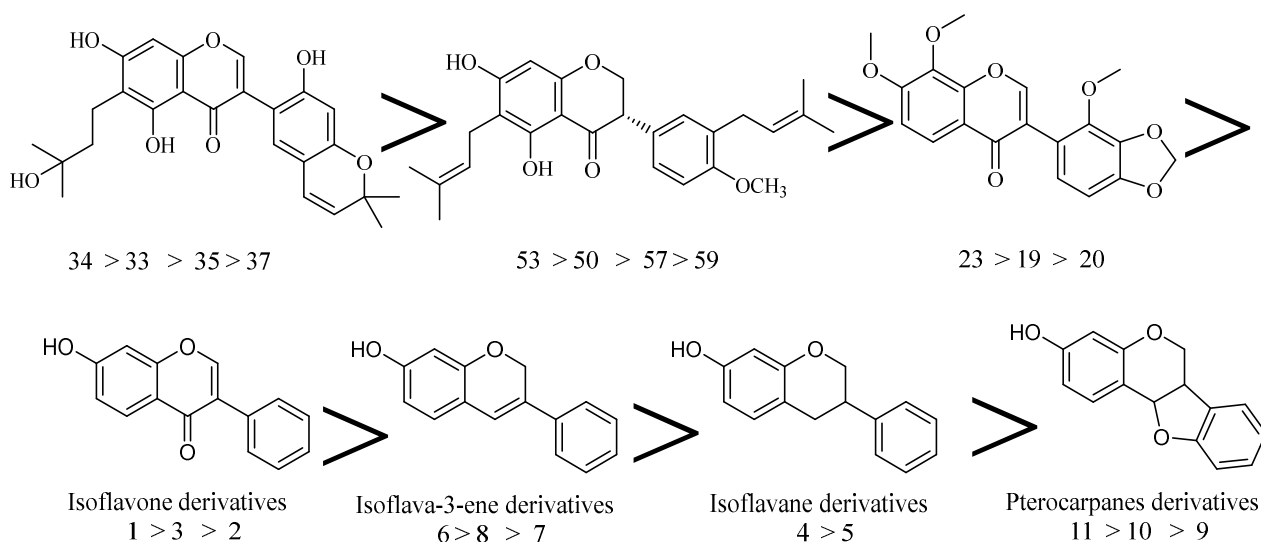


Figure 15. Schematic diagram showing the different affinities of isoflavonoids against hACE-2.

For isoflavone derivatives (compounds 34, 33, 35 and 37), it was found that compound 34 incorporating 3-hydroxy-3-methylbutyl moiety at 6-position was more active than compound 33 incorporating 3-methylbut-2-en-1-yl moiety at the same position. The latter was more active than compound 35 incorporating 2-hydroxy-3-methylbut-3-en-1-yl moiety at the same position. Compound 37 incorporating 3-methylbut-2-en-1-yl moiety at 8-position was less active than the corresponding members.

With regard to isoflavane derivatives (compounds 50, 53, 57 and 59), it was found that 3-methylbut-2-en-1-yl moiety is critical for binding affinity. compound 50 incorporating this moiety at 3- and 6-positions of 4-chromanone nucleus was more active than compound 53 incorporating this moiety at 5-position of phenyl ring. The latter was more active than compound 57 incorporating 3-methylbut-2-en-1-yl moiety at both 6-position position of 4-chromanone nucleus and 3-position of phenyl ring. Compound 59 incorporating 3-methylbut-2-en-1-yl moiety at both 8-position position of 4-chromanone nucleus and 3-position of phenyl ring was less active than the corresponding members.

Regarding isoflavone derivatives (compounds 19, 20, and 23), it was found that the presence of 1,3-dioxole moiety can affect the affinity depending on its position. compound 19 incorporating 1,3-dioxole moiety at 3,4-positions of phenyl ring was more active than compound 20 incorporating this moiety at 7,8-position of 4H-chromen-4-one nucleus. The latter was more active than compound 23 incorporating 1,3-dioxole moiety at 4,5-position position of phenyl ring.

Then, we investigated the effect of substitutions at isoflavone derivatives on the binding affinity. It was found that the substitutions at 5-position with hydroxyl (compound 1) and methoxy (compound 3) group, increase the binding of isoflavones against hACE-2, with an increased affinity of hydroxyl derivative.

Regarding the effect of substitutions at isoflava-3-ene, it was found that the derivative with additional pyran ring (compound 6) was more active than the corresponding member with free OH group at position-1 of phenyl ring (compound 8) which was more potent than compound 7 incorporating a dioxolan ring.

Observing binding affinities of isoflavane derivatives. It was found that compound 4 incorporating an additional methoxy group at 6 position of phenyl ring showed better binding affinity against hACE-2 than the unsubstituted derivative (compound 5). Such a result may be attributed to the electron donating effect of the methoxy group.

Concerning the activity of different pterocarpan derivatives, it was noted that compound **11**, which contained an additional tetrahydrofuran ring attached to the chromene ring, showed better binding affinity inside the hACE-2 than compounds **9** and **10**, which contained free OH groups at the chromene ring.

3.3. Toxicity Studies

Toxicity prediction was carried out based on the validated and constructed models in *Discovery studio 4.0* software [49,50] as follows. (i) FDA rodent carcinogenicity test which computes the probability of a compound to be a carcinogen. (ii) Carcinogenic potency TD_{50} which predicts the tumorigenic dose rate 50 (TD_{50}) of a drug in a rodent chronic exposure toxicity test of carcinogenic potency [51]. (iii) Rat maximum tolerated dose (MTD) [52,53]. (iv) Rat oral LD_{50} which predicts the rat oral acute median lethal dose (LD_{50}) of a chemical [54]. (v) Rat chronic LOAEL which predicts the rat chronic lowest observed adverse effect level (LOAEL) value [55,56]. (vi) Ocular irritancy predicts whether a particular compound is likely to be an ocular irritant and how severe the irritation is in the Draize test [57]. (vii) Skin irritancy predicts whether a particular compound is likely to be a skin irritant and how severe it is in a rabbit skin irritancy test [57].

As shown in Table 5, most compounds showed in silico low toxicity against the tested models. FDA rodent carcinogenicity model indicated that most of the tested compounds are non-carcinogens. Only compounds **6**, **9**, and **10** were predicted to be carcinogens so that, these compounds do not have the likeness to be used as drugs.

Table 5. Toxicity properties of isoflavonoids (1–59) and semiprever.

Comp.	FDA Rodent Carcinogenicity	Carcinogenic Potency TD_{50} (Rat) ^a	Rat MTD (Feed) ^b	Rat Oral LD_{50} ^c	Rat Chronic LOAEL ^d	Ocular Irritancy	Skin Irritancy
1	Non-Carcinogen	60.47	0.516	1.40	0.107	Irritant	None
2	Non-Carcinogen	67.14	0.334	1.41	0.089	Irritant	None
3	Non-Carcinogen	10.43	0.225	0.81	0.068	Irritant	None
4	Non-Carcinogen	5.69	0.231	0.17	0.072	Irritant	None
5	Non-Carcinogen	5.73	0.234	0.17	0.071	Irritant	None
6	Carcinogen	35.33	0.239	0.77	0.024	Irritant	None
7	Non-Carcinogen	6.23	0.096	0.48	0.019	Irritant	None
8	Non-Carcinogen	33.45	0.529	1.06	0.074	Irritant	Mild
9	Carcinogen	4.43	0.122	0.14	0.027	Irritant	Mild
10	Carcinogen	28.52	0.126	0.16	0.011	Irritant	None
11	Non-Carcinogen	7.51	0.192	0.55	0.015	Irritant	None
12	Non-Carcinogen	193.96	0.078	0.10	0.004	Mild	None
13	Non-Carcinogen	5.27	0.255	1.07	0.865	Mild	None
14	Non-Carcinogen	9.10	0.164	1.13	0.325	Mild	None
15	Non-Carcinogen	7.32	0.288	2.03	0.147	Mild	None
16	Non-Carcinogen	7.91	0.230	1.67	0.155	Mild	None
17	Non-Carcinogen	8.98	0.184	1.18	0.152	None	None
18	Non-Carcinogen	8.40	0.205	1.69	0.309	Mild	None
19	Non-Carcinogen	0.77	0.069	0.39	0.130	None	Mild
20	Non-Carcinogen	0.59	0.061	0.20	0.145	None	Mild
21	Non-Carcinogen	6.40	0.181	1.44	0.229	Mild	None
22	Non-Carcinogen	5.73	0.205	2.36	0.390	Mild	None
23	Non-Carcinogen	0.44	0.077	0.42	0.282	Mild	Mild
24	Non-Carcinogen	6.88	0.288	4.66	0.863	Mild	None
25	Non-Carcinogen	19.50	0.181	0.97	0.191	None	None
26	Non-Carcinogen	10.75	0.145	1.01	0.281	Mild	None
27	Non-Carcinogen	29.81	0.184	1.74	0.054	Mild	None
28	Non-Carcinogen	19.03	0.199	0.77	0.035	None	None
29	Non-Carcinogen	25.03	0.080	0.35	0.055	Severe	None
30	Non-Carcinogen	2.33	0.097	0.45	0.039	Severe	None
31	Non-Carcinogen	2.33	0.097	0.45	0.039	Severe	None
32	Non-Carcinogen	20.46	0.128	0.26	0.074	Mild	None

Table 5. Cont.

Comp.	FDA Rodent Carcinogenicity	Carcinogenic Potency TD ₅₀ (Rat) ^a	Rat MTD (Feed) ^b	Rat Oral LD ₅₀ ^c	Rat Chronic LOAEL ^d	Ocular Irritancy	Skin Irritancy
33	Non-Carcinogen	73.66	0.197	0.29	0.013	Mild	Mild
34	Non-Carcinogen	25.44	0.526	0.92	0.018	Severe	None
35	Non-Carcinogen	6.87	0.236	0.37	0.013	Mild	None
36	Non-Carcinogen	322.42	0.764	0.84	0.029	Severe	None
37	Non-Carcinogen	165.35	0.303	1.39	0.008	Mild	None
38	Non-Carcinogen	19.21	0.153	0.46	0.024	Mild	None
39	Non-Carcinogen	35.43	0.576	0.70	0.012	Severe	None
40	Non-Carcinogen	4.926	0.216	0.44	0.015	Mild	None
41	Non-Carcinogen	6.31	0.381	0.98	0.075	Severe	None
42	Non-Carcinogen	5.95	0.428	0.71	0.026	Mild	None
43	Non-Carcinogen	6.31	0.381	0.91	0.044	Mild	None
44	Non-Carcinogen	5.81	0.475	1.12	0.041	Mild	None
45	Non-Carcinogen	5.28	0.402	0.76	0.037	Mild	None
46	Non-Carcinogen	3.25	0.668	1.10	0.174	Mild	None
47	Non-Carcinogen	4.02	0.395	0.65	0.084	None	None
48	Non-Carcinogen	126.90	0.545	0.39	0.009	Severe	None
49	Non-Carcinogen	14.44	0.284	0.32	0.024	Mild	None
50	Non-Carcinogen	14.44	0.284	0.20	0.008	Mild	None
51	Non-Carcinogen	16.34	0.226	0.14	0.008	Mild	None
52	Non-Carcinogen	21.43	0.226	0.46	0.010	Mild	None
53	Non-Carcinogen	18.79	0.150	0.34	0.008	Mild	None
54	Non-Carcinogen	18.79	0.150	0.26	0.007	Mild	None
55	Non-Carcinogen	14.61	0.226	0.32	0.053	Severe	None
56	Non-Carcinogen	116.75	0.562	0.42	0.006	Severe	None
57	Non-Carcinogen	177.62	0.291	0.36	0.004	Severe	None
58	Non-Carcinogen	5.28	0.156	0.18	0.016	Mild	None
59	Non-Carcinogen	15.21	0.208	0.35	0.014	Mild	None
Simeprevir	Non-Carcinogen	0.28	0.003	0.21	0.002	Irritant	None

^a TD₅₀, tumorigenic dose rate 50, Unit: mg kg⁻¹ body weight/day; ^b MTD, maximum tolerated dose, Unit: g kg⁻¹ body weight; ^c LD₅₀, median lethal dose, Unit: g kg⁻¹ body weight; ^d LOAEL, lowest observed adverse effect level, Unit: g kg⁻¹ body weight.

For the carcinogenic potency TD₅₀ rat model, the examined compounds showed TD₅₀ values ranging from 0.44 to 322.42 mg Kg⁻¹ body weight/day which are higher than simeprevir (0.280 mg Kg⁻¹ body weight/day).

Regarding the rat MTD model, the compounds showed MTD with a range of 0.061 to 0.764 g kg⁻¹ body weight higher than simeprevir (0.003 g kg⁻¹ body weight).

Concerning the rat oral LD₅₀ model, the tested compounds showed oral LD₅₀ values ranging from 0.10 to 4.66 mg Kg⁻¹ body weight/day, while simeprevir exhibited an oral LD₅₀ value of 0.21 mg Kg⁻¹ body weight/day. About the rat chronic LOAEL model, the compounds showed LOAEL values ranging from 0.004 to 0.865 g kg⁻¹ body weight. These values are higher than simeprevir (0.002 g kg⁻¹ body weight). Moreover, most of the compounds were predicted to be irritant against the ocular irritancy model. On the other hand, the tested compounds were predicted to be mild or non-irritant against the skin irritancy model.

4. Conclusions

There is an urgent global need to find a cure for COVID-19. The present work is an attempt to find some natural compounds with potential activity against COVID-19. Accordingly, docking studies were carried out for fifty-nine isoflavonoid derivatives against two essential targets (hACE-2 and M^{Pro}). The obtained results showed that the tested isoflavonoids can strongly bind the hACE-2 and M^{Pro} with great binding modes. Based on in silico studies, SARs were established. SAR studies afforded an insight into the pharmacophoric groups which may serve as a guide for the design of new potential anti-

COVID-19 agents. Generally, the tested compounds showed decreased affinity against hACE-2 in descending order of isoflavone derivatives (compounds 33–35 and 37) > isoflavane derivatives (compounds 50, 53, 57 and 59) > isoflavone derivatives (compounds 19, 20 and 23) > isoflavone derivatives (compounds 1–3) > isoflavan-3-ene derivatives (compounds 6–8) > isoflavane derivatives (compounds 4 and 5) > pterocarpan derivatives (compounds 9–11) Finally, compounds 33 and 56 showed the most acceptable affinity against hACE2; compounds 30 and 53 showed the best docking results against M^{Pro}. In addition, these compounds showed good physicochemical and cytotoxicity profiles. Moreover, in silico investigation of physicochemical properties, ADMET and toxicity studies revealed good properties and general low toxicity. Consequently, this study strongly suggests in vitro and in vivo studies for the most active isoflavonoids against COVID-19.

Author Contributions: M.S.A.: docking studies, A.E.A.: Data curation and Writing the original draft, M.S.T.: Writing original draft, E.B.E.: Resources, I.H.E.: ADMET and toxicity studies, A.M.M.: Writing-review & editing. I.H.E. and A.M.M.: Designed the idea and supervised the work. All authors have read and agreed to the published version of the manuscript.

Funding: This research received no external funding and The APC was funded by AlMaarefa University, Ad Diriyah, Riyadh 13713, Saudi Arabia.

Institutional Review Board Statement: Not applicable.

Informed Consent Statement: Not applicable.

Data Availability Statement: Not applicable.

Acknowledgments: The authors acknowledge Faculty of Pharmacy (Boys), Al-Azhar University, Cairo, Egypt for computer supply.

Conflicts of Interest: The authors declare no conflict of interest.

Sample Availability: Samples of the compounds are not available from the authors.

References

1. Zumla, A.; Chan, J.F.; Azhar, E.I.; Hui, D.S.; Yuen, K.Y. Coronaviruses - drug discovery and therapeutic options. *Nat. Rev. Drug Discov.* **2016**, *15*, 327–347. [[CrossRef](#)] [[PubMed](#)]
2. Su, S.; Wong, G.; Shi, W.; Liu, J.; Lai, A.C.K.; Zhou, J.; Liu, W.; Bi, Y.; Gao, G.F. Epidemiology, Genetic Recombination, and Pathogenesis of Coronaviruses. *Trends Microbiol.* **2016**, *24*, 490–502. [[CrossRef](#)]
3. WHO. WHO Coronavirus Disease (COVID-19) Dashboard. Available online: <https://covid19.who.int/> (accessed on 2 October 2020).
4. Dolin, R.; Hirsch, M.S. *Remdesivir—An Important First Step*; Massachusetts Medical Society: Waltham, MA, USA, 2020.
5. Zhang, L.; Lin, D.; Sun, X.; Curth, U.; Drosten, C.; Sauerhering, L.; Becker, S.; Rox, K.; Hilgenfeld, R. Crystal structure of SARS-CoV-2 main protease provides a basis for design of improved α -ketoamide inhibitors. *Science* **2020**, *368*, 409–412. [[CrossRef](#)] [[PubMed](#)]
6. Prajapat, M.; Sarma, P.; Shekhar, N.; Avti, P.; Sinha, S.; Kaur, H.; Kumar, S.; Bhattacharyya, A.; Kumar, H.; Bansal, S. Drug targets for corona virus: A systematic review. *Indian J. Pharmacol.* **2020**, *52*, 56.
7. Riordan, J.F. Angiotensin-I-converting enzyme and its relatives. *Genome Biol.* **2003**, *4*, 1–5. [[CrossRef](#)] [[PubMed](#)]
8. Ichihara, K.I.; Fukubayashi, Y. Preparation of fatty acid methyl esters for gas-liquid chromatography. *J. Lipid Res.* **2010**, *51*, 635–640. [[CrossRef](#)]
9. Ksiazek, T.G.; Erdman, D.; Goldsmith, C.S.; Zaki, S.R.; Peret, T.; Emery, S.; Tong, S.; Urbani, C.; Comer, J.A.; Lim, W. A novel coronavirus associated with severe acute respiratory syndrome. *New Engl. J. Med.* **2003**, *348*, 1953–1966. [[CrossRef](#)] [[PubMed](#)]
10. Harmer, D.; Gilbert, M.; Borman, R.; Clark, K.L. Quantitative mRNA expression profiling of ACE 2, a novel homologue of angiotensin converting enzyme. *FEBS Lett.* **2002**, *532*, 107–110. [[CrossRef](#)]
11. Yan, R.; Zhang, Y.; Li, Y.; Xia, L.; Guo, Y.; Zhou, Q. Structural basis for the recognition of SARS-CoV-2 by full-length human ACE2. *Science* **2020**, *367*, 1444–1448. [[CrossRef](#)]
12. Tortorici, M.A.; Veesler, D. Structural insights into coronavirus entry. In *Advances in Virus Research*; Elsevier: Amsterdam, The Netherlands, 2019; Volume 105, pp. 93–116.
13. Yang, J.; Petitjean, S.J.; Koehler, M.; Zhang, Q.; Dumitru, A.C.; Chen, W.; Derclaye, S.; Vincent, S.P.; Soumillion, P.; Alsteens, D. Molecular interaction and inhibition of SARS-CoV-2 binding to the ACE2 receptor. *Nat. Commun.* **2020**, *11*, 1–10. [[CrossRef](#)]
14. Zhang, H.; Penninger, J.M.; Li, Y.; Zhong, N.; Slutsky, A.S. Angiotensin-converting enzyme 2 (ACE2) as a SARS-CoV-2 receptor: Molecular mechanisms and potential therapeutic target. *Intensive Care Med.* **2020**, *46*, 586–590. [[CrossRef](#)] [[PubMed](#)]

15. Jia, H.P.; Look, D.C.; Shi, L.; Hickey, M.; Pewe, L.; Netland, J.; Farzan, M.; Wohlford-Lenane, C.; Perlman, S.; McCray, P.B. ACE2 receptor expression and severe acute respiratory syndrome coronavirus infection depend on differentiation of human airway epithelia. *J. Virol.* **2005**, *79*, 14614–14621. [[CrossRef](#)] [[PubMed](#)]
16. Metwaly, A.M.; Lianlian, Z.; Luqi, H.; Deqiang, D. Black ginseng and its saponins: Preparation, phytochemistry and pharmacological effects. *Molecules* **2019**, *24*, 1856. [[CrossRef](#)]
17. Wang, Y.-M.; Ran, X.-K.; Riaz, M.; Yu, M.; Cai, Q.; Dou, D.-Q.; Metwaly, A.M.; Kang, T.-G.; Cai, D.-C. Chemical Constituents of Stems and Leaves of *Tagetespatula* L. and Its Fingerprint. *Molecules* **2019**, *24*, 3911. [[CrossRef](#)] [[PubMed](#)]
18. Sperstad, S.V.; Haug, T.; Blencke, H.-M.; Styrvold, O.B.; Li, C.; Stensvåg, K. Antimicrobial peptides from marine invertebrates: Challenges and perspectives in marine antimicrobial peptide discovery. *Biotechnol. Adv.* **2011**, *29*, 519–530. [[CrossRef](#)]
19. El-Demerdash, A.; Metwaly, A.M.; Hassan, A.; El-Aziz, A.; Mohamed, T.; Elkaeed, E.B.; Eissa, I.H.; Arafa, R.K.; Stockand, J.D. Comprehensive Virtual Screening of the Antiviral Potentialities of Marine Polycyclic Guanidine Alkaloids against SARS-CoV-2 (Covid-19). *Biomolecules* **2021**, *11*, 460. [[CrossRef](#)]
20. Metwaly, A.M.; Wanas, A.S.; Radwan, M.M.; Ross, S.A.; ElSohly, M.A. New α -Pyrone derivatives from the endophytic fungus *Embellisia* sp. *Med. Chem. Res.* **2017**, *26*, 1796–1800. [[CrossRef](#)]
21. Metwaly, A.; Kadry, H.; El-Hela, A.; Elsalam, A.; Ross, S. New antimalarial benzopyran derivatives from the endophytic fungus *Alternaria phragmospora*. *Planta Med.* **2014**, *80*, PC11. [[CrossRef](#)]
22. Metwaly, A. Comparative biological evaluation of four endophytic fungi isolated from *nigella sativa* seeds. *Al-Azhar J. Pharm. Sci.* **2019**, *59*, 123–136. [[CrossRef](#)]
23. Yassin, A.M.; El-Deeb, N.M.; Metwaly, A.M.; El Fawal, G.F.; Radwan, M.M.; Hafez, E.E. Induction of apoptosis in human cancer cells through extrinsic and intrinsic pathways by *Balanites aegyptiaca* furostanol saponins and saponin-coated silvernanoparticles. *Appl. Biochem. Biotechnol.* **2017**, *182*, 1675–1693. [[CrossRef](#)]
24. Sharaf, M.H.; El-Sherbiny, G.M.; Moghannem, S.A.; Abdelmonem, M.; Elsehemy, I.A.; Metwaly, A.M.; Kalaba, M.H. New combination approaches to combat methicillin-resistant *Staphylococcus aureus* (MRSA). *Sci. Rep.* **2021**, *11*, 1–16. [[CrossRef](#)] [[PubMed](#)]
25. Metwaly, A.M.; Ghoneim, M.M.; Musa, A. Two new antileishmanial diketopiperazine alkaloids from the endophytic fungus *Trichosporum* sp. *Derpharmachemica* **2015**, *7*, 322–327.
26. Metwaly, A.M.; Fronczek, F.R.; Ma, G.; Kadry, H.A.; Atef, A.; Mohammad, A.-E.I.; Cutler, S.J.; Ross, S.A. Antileukemic α -pyrone derivatives from the endophytic fungus *Alternaria phragmospora*. *Tetrahedron Lett.* **2014**, *55*, 3478–3481. [[CrossRef](#)] [[PubMed](#)]
27. Metwaly, A.M.; Kadry, H.A.; Atef, A.; Mohammad, A.-E.I.; Ma, G.; Cutler, S.J.; Ross, S.A. Nigrosphaerin A a new isochromene derivative from the endophytic fungus *Nigrospora sphaerica*. *Phytochem. Lett.* **2014**, *7*, 1–5. [[CrossRef](#)] [[PubMed](#)]
28. Zhazhaxina, A.; Suleimen, Y.; Metwaly, A.M.; Eissa, I.H.; Elkaeed, E.B.; Suleimen, R.; Ishmuratova, M.; Akatan, K.; Luyten, W. In Vitro and In Silico Cytotoxic and Antibacterial Activities of a Diterpene from *Cousinia alata* Schrenk. *J. Chem.* **2021**, *2021*. [[CrossRef](#)]
29. Ghoneim, M.M.; Afifi, W.M.; Ibrahim, M.; Elagawany, M.; Khayat, M.T.; Aboutaleb, M.H.; Metwaly, A.M. Biological evaluation and molecular docking study of metabolites from *Salvadora Persica* L. Growing in Egypt. *Pharmacogn. Mag.* **2019**, *15*, 232.
30. Hegazy, M.M.; Metwaly, A.M.; Mostafa, A.E.; Radwan, M.M.; Mehany, A.B.M.; Ahmed, E.; Enany, S.; Magdeldin, S.; Afifi, W.M.; ElSohly, M.A. Biological and chemical evaluation of some African plants belonging to *Kalanchoe* species: Antitrypanosomal, cytotoxic, antitopoisomerase I activities and chemical profiling using ultra-performance liquid chromatography/quadrupole-time-of-flight mass spectrometer. *Pharmacogn. Mag.* **2021**, *17*, 6.
31. Orazbekov, Y.; Datkhayev, U.; Omyrzakov, M.; Metwaly, A.; Makhatov, B.; Jacob, M.; Ramazanov, B.; Sakipova, Z.; Azembayev, A.; Orazbekuly, K. Antifungal prenylated isoflavonoids from *Maclura aurantiaca*. *Planta Med.* **2015**, *81*, PE10. [[CrossRef](#)]
32. Dewick, P.M. Isoflavonoids. In *The Flavonoids: Advances in Research since 1980*, Harborne, J.B., Ed.; Springer US: Boston, MA, USA, 1988; pp. 125–209.
33. Arthan, D.; Svasti, J.; Kittakoop, P.; Pittayakhachonwut, D.; Tanticharoen, M.; Thebtaranonth, Y. Antiviral isoflavonoid sulfate and steroidal glycosides from the fruits of *Solanum torvum*. *Phytochemistry* **2002**, *59*, 459–463. [[CrossRef](#)]
34. Okubo, K.; Kudou, S.; Uchida, T.; Yoshiki, Y.; Yoshikoshi, M.; Tonomura, M. Soybean Saponin and Isoflavonoids. In *Food Phytochemicals for Cancer Prevention I*; American Chemical Society: Washington, DC, USA, 1993; Volume 546, pp. 330–339.
35. Horio, Y.; Sogabe, R.; Shichiri, M.; Ishida, N.; Morimoto, R.; Ohshima, A.; Isegawa, Y. Induction of a 5-lipoxygenase product by daidzein is involved in the regulation of influenza virus replication. *J. Clin. Biochem. Nutr.* **2020**, *66*, 36–42. [[CrossRef](#)]
36. Tait, S.; Salvati, A.L.; Desideri, N.; Fiore, L. Antiviral activity of substituted homoisoflavonoids on enteroviruses. *Antivir. Res.* **2006**, *72*, 252–255. [[CrossRef](#)] [[PubMed](#)]
37. Desideri, N.; Olivieri, S.; Stein, M.; Sgro, R.; Orsi, N.; Conti, C. Synthesis and anti-picornavirus activity of homo-isoflavonoids. *Antivir. Chem. Chemother.* **1997**, *8*, 545–555. [[CrossRef](#)]
38. Lipinski, C.A.; Lombardo, F.; Dominy, B.W.; Feeney, P.J. Experimental and computational approaches to estimate solubility and permeability in drug discovery and development settings. *Adv. Drug Deliv. Rev.* **1997**, *23*, 3–25. [[CrossRef](#)]
39. BIOVIA. *Discovery Studio Visualizer*; BIOVIA: San Diego, CA, USA, 2012; Available online: <https://discover.3ds.com/discovery-studio-visualizer-download> (accessed on 22 March 2021).
40. Bank. 2020. Available online: <https://www.rcsb.org/structure/6LZG> (accessed on 2 January 2021).
41. Bank. 2020. Available online: <https://www.rcsb.org/structure/6LU7> (accessed on 2 January 2020).

42. Ibrahim, M.K.; Eissa, I.H.; Abdallah, A.E.; Metwaly, A.M.; Radwan, M.; ElSohly, M. Design, synthesis, molecular modeling and anti-hyperglycemic evaluation of novel quinoxaline derivatives as potential PPAR γ and SUR agonists. *Bioorganic Med. Chem.* **2017**, *25*, 1496–1513. [[CrossRef](#)] [[PubMed](#)]
43. El-Helby, A.G.A.; Ayyad, R.R.; Sakr, H.M.; Abdelrahim, A.S.; El-Adl, K.; Sherbiny, F.S.; Eissa, I.H.; Khalifa, M.M. Design, synthesis, molecular modeling and biological evaluation of novel 2, 3-dihydrophthalazine-1, 4-dione derivatives as potential anticonvulsant agents. *J. Mol. Struct.* **2017**, *1130*, 333–351. [[CrossRef](#)]
44. Ibrahim, M.K.; Eissa, I.H.; Alesawy, M.S.; Metwaly, A.M.; Radwan, M.M.; ElSohly, M.A. Design, synthesis, molecular modeling and anti-hyperglycemic evaluation of quinazolin-4 (3H)-one derivatives as potential PPAR γ and SUR agonists. *Bioorganic Med. Chem.* **2017**, *25*, 4723–4744. [[CrossRef](#)]
45. Eissa, I.H.; Metwaly, A.M.; Belal, A.; Mehany, A.B.; Ayyad, R.R.; El-Adl, K.; Mahdy, H.A.; Taghour, M.S.; El-Gamal, K.M.; El-Sawah, M.E. Discovery and antiproliferative evaluation of new quinoxalines as potential DNA intercalators and topoisomerase II inhibitors. *Arch. Der Pharm.* **2019**, *352*, 1900123. [[CrossRef](#)] [[PubMed](#)]
46. PerkinElmer. *ChemBioDraw Ultra 14.0*; PerkinElmer: Waltham, MA, USA, 2012; Available online: <https://shopinformatics.perkinelmer.com/search> (accessed on 2 May 2015).
47. El-Gamal, K.M.; El-Morsy, A.M.; Saad, A.M.; Eissa, I.H.; Alswah, M. Synthesis, docking, QSAR, ADMET and antimicrobial evaluation of new quinoline-3-carbonitrile derivatives as potential DNA-gyrase inhibitors. *J. Mol. Struct.* **2018**, *1166*, 15–33. [[CrossRef](#)]
48. El-Zahabi, M.A.; Elbendary, E.R.; Bamanie, F.H.; Radwan, M.F.; Ghareib, S.A.; Eissa, I.H. Design, synthesis, molecular modeling and anti-hyperglycemic evaluation of phthalimide-sulfonylurea hybrids as PPAR γ and SUR agonists. *Bioorganic Chem.* **2019**, *91*, 103115. [[CrossRef](#)]
49. Xia, X.; Maliski, E.G.; Gallant, P.; Rogers, D. Classification of kinase inhibitors using a Bayesian model. *J. Med. Chem.* **2004**, *47*, 4463–4470. [[CrossRef](#)] [[PubMed](#)]
50. BIOVIA. QSAR, ADMET and Predictive Toxicology. Available online: <https://www.3dsbiovia.com/products/collaborative-science/biovia-discovery-studio/qsar-admet-and-predictive-toxicology.html> (accessed on 15 May 2020).
51. Venkatapathy, R.; Wang, N.C.Y.; Martin, T.M.; Harten, P.F.; Young, D. Structure–Activity Relationships for Carcinogenic Potential. *Gen. Appl. Syst. Toxicol.* **2009**. [[CrossRef](#)]
52. Goodrnan, G.; Wilson, R. Comparison of the dependence of the TD50 on maximum tolerated dose for mutagens and nonmutagens. *Risk Anal.* **1992**, *12*, 525–533. [[CrossRef](#)] [[PubMed](#)]
53. Council, N.R. Correlation Between Carcinogenic Potency and the Maximum Tolerated Dose: Implications for Risk Assessment. In *Issues in Risk Assessment*; National Academies Press (US): Cambridge, MA, USA, 1993.
54. Gonella Diaza, R.; Manganelli, S.; Esposito, A.; Roncaglioni, A.; Manganaro, A.; Benfenati, E. Comparison of in silico tools for evaluating rat oral acute toxicity. *Sar Qsar Environ. Res.* **2015**, *26*, 1–27. [[CrossRef](#)] [[PubMed](#)]
55. Pizzo, F.; Benfenati, E. In silico models for repeated-dose toxicity (RDT): Prediction of the no observed adverse effect level (NOAEL) and lowest observed adverse effect level (LOAEL) for drugs. In *In Silico Methods for Predicting Drug Toxicity*; Springer: Berlin/Heidelberg, Germany, 2016; pp. 163–176.
56. Venkatapathy, R.; Moudgal, C.J.; Bruce, R.M. Assessment of the oral rat chronic lowest observed adverse effect level model in TOPKAT, a QSAR software package for toxicity prediction. *J. Chem. Inf. Comput. Sci.* **2004**, *44*, 1623–1629. [[CrossRef](#)] [[PubMed](#)]
57. Wilhelmus, K.R. The Draize eye test. *Surv. Ophthalmol.* **2001**, *45*, 493–515. [[CrossRef](#)]